NASA MEMO 4-30-59L

NASA

MEMORANDUM

TRANSONIC AERODYNAMIC CHARACTERISTICS OF TWO WEDGE AIRFOIL SECTIONS INCLUDING UNSTEADY FLOW STUDIES

By Patrick J. Johnston

Langley Research Center
Langley Field, Va.

NATIONAL AERONAUTICS AND SPACE ADMINISTRATION

WASHINGTON

June 1959

NATIONAL AERONAUTICS AND SPACE ADMINISTRATION

MEMORANDUM 4-30-59L

TRANSONIC AERODYNAMIC CHARACTERISTICS OF TWO WEDGE AIRFOIL SECTIONS INCLUDING UNSTEADY FLOW STUDIES*

By Patrick J. Johnston

SUMMARY

A two-dimensional wind-tunnel investigation has been conducted on a 20-percent-thick single-wedge airfoil section. Steady-state forces and moments were determined from pressure measurements at Mach numbers from 0.70 to about 1.25. Additional information on the flows about the single wedge is provided by means of instantaneous pressure measurements at Mach numbers up to unity. Pressure distributions were also obtained on a symmetrical double-wedge or diamond-shaped profile which had the same leading-edge included angle as the single-wedge airfoil. A comparison of the data on the two profiles to provide information on the effects of the afterbody showed that with the exception of drag, the single-wedge profile proved to be aerodynamically superior to the diamond profile in all respects.

The lift effectiveness of the single-wedge airfoil section far exceeded that of conventional thin airfoil sections over the speed range of the investigation. Pitching-moment irregularities, caused by negative loadings near the trailing edge, generally associated with conventional airfoils of equivalent thicknesses were not exhibited by the single-wedge profile.

Moderately high pulsating pressures existing over the base of the single-wedge airfoil section were significantly reduced as the Mach number was increased beyond 0.92 and the boundaries of the dead airspace at the base of the model converged to eliminate the vortex street in the wake.

Increasing the leading-edge radius from 0 to 1 percent of the chord had a minor effect on the steady-state forces and generally raised the level of pressure pulsations over the forward part of the single-wedge profile.

INTRODUCTION

Supersonic theory indicates a rapid loss in lift-curve slope of airfoils as high Mach numbers are approached. At hypersonic speeds, therefore, adequate stability and control may be difficult to obtain. In order to overcome this deficiency in lift effectiveness, one theoretical proposal (ref. 1) suggests the substitution of simple wedge-type airfoils having blunt trailing edges in place of conventional thin profiles used as control surfaces. Aerodynamic heating problems at high Mach numbers might require that their sharp leading edges be rounded.

Even though the single-wedge profile appears desirable as a control surface for hypersonic speeds, it is also of interest to study its aerodynamic characteristics at transonic speeds since the flight patterns of some hypersonic vehicles might extend into the transonic and subsonic speed range.

Information on wedge-type airfoils at transonic speeds is limited almost exclusively to the symmetrical double-wedge (designated diamond herein) profiles. (See refs. 2 to 6.) In one investigation a single-wedge section was tested in conjunction with a flat-plate extension at zero lift (ref. 7). Two investigations (refs. 8 and 9) have included tests of single wedges in subsonic, closed-throat wind tunnels. Maximum Mach numbers and/or angles of attack obtained in the tests of references 8 and 9 were limited, however, due to tunnel choking.

Since little information is available at Mach numbers near unity and the single wedge appears potentially useful as a high Mach number profile, a transonic wind-tunnel investigation was conducted to determine the force and moment characteristics of a 20-percent-thick single-wedge profile in the Mach number range from 0.70 to 1.25 and angles of attack up to 8°. The results are compared with those obtained on a diamond airfoil having the same leading-edge included angle. Effects of leading-edge bluntness at transonic speeds were investigated by rounding the nose of the single wedge to radii of 0.5 and 1.0 percent of the chord. Measurements were also made of the unsteady flow characteristics of the single wedge for each leading-edge condition.

SYMBOLS

c_d section pressure-drag coefficient

c_n section normal-force coefficient

$c_{m,le}$ section pitching-moment coefficient about leading edge

c_{n_α} section normal-force curve slope

C_p pressure coefficient

d pressure drag

M Mach number

n section normal force

Δp double-amplitude pressure pulsation

q dynamic pressure

r leading-edge radius, percent chord

x_{cp} location of center of pressure in percent chord from leading edge

α angle of attack

Subscripts:

b base

cr critical (local M = 1)

f forebody

max maximum

t total

APPARATUS, MODELS, AND TESTS

Wind Tunnels

Pressure-distribution investigations were conducted in the Langley airfoil test apparatus (ref. 10), a transonic blowdown tunnel, whose test section is 4 inches wide by 19 inches high (fig. 1). A calibration of the test region indicated the stream Mach numbers to be satisfactorily uniform, having a maximum variation of ±0.002 in the horizontal plane and about ±0.010 in the vertical. Schlieren flow studies and pressure measurements showed that, at low supersonic speeds, the bow shock wave reflections had no effect on the data. When the disturbances produced

by the reflected shock were directed back toward the tunnel center line at somewhat higher Mach numbers, the disturbances crossed the model wake well downstream of the trailing edge.

Stagnation pressure was held constant at 26 psia for all the tests. The stream Mach number was controlled by regulating the mass flow through the variable area choker section downstream of the test section. A more complete description of this tunnel may be found in reference 10.

Pressure pulsation and schlieren data were obtained in the Langley 4- by 19-inch semiopen tunnel, reference 11, operating as a blowdown facility at a stagnation pressure of 26 psia. Results presented in reference 10 show that the data obtained from the two facilities obtained under the same operating conditions are in agreement; hence, a close similarity of the flows about the models will exist. The two primary reasons for using the Langley 4- by 19-inch semiopen tunnel for the pressure pulsation tests were: (1) ease of installation of pressure measuring equipment (the test section is not surrounded by a plenum chamber) and (2) pressure pulsations would cease above a Mach number of one, and Mach numbers up to one were obtainable in this tunnel.

Models

The 20-percent-thick wedge airfoil had a 2-inch chord and completely spanned the 4-inch width of the tunnel. Eighteen static pressure orifices were located at 0.2-inch intervals along the upper and lower surfaces near the midspan of the model. An additional orifice was installed on the chord line at the rear of the model to measure base pressure. Leading-edge bluntness was incorporated into the model by rounding the sharp nose to a 0.5-percent-chord leading-edge radius and finally to a 1.0-percent-chord leading-edge radius.

Six orifices were installed in the model for the unsteady flow investigation. In addition to one orifice on the base, the remaining orifices were arbitrarily located at the 25-, 50-, 75-, and 96-percent-chord stations along the upper surface and at the 96-percent-chord station on the lower surface. Instrumentation for these tests was the same as that described in reference 12.

Tests were also conducted on a 4-inch-chord, 10-percent-chord-thick, symmetrical double-wedge or diamond airfoil. Static pressure orifices were located at 5-percent-chord intervals along both upper and lower surfaces of this model beginning at the 5-percent-chord location. The leading edge of this model was sharp and was not altered during the tests.

Tests

Pressure-distribution tests and schlieren observations were made for the airfoils at angles of attack from 0° to 8° in 2° increments. The data were obtained at Mach number increments of 0.025 although generally only those data at Mach number increments of 0.05 were reduced to coefficient form. Reynolds numbers, for a stagnation pressure of 26 psia, ranged from 1.2×10^6 to 1.4×10^6 based on the 2-inch-chord length of the single-wedge model.

PRESENTATION OF RESULTS

Flow characteristics, in the form of schlieren photographs, are presented in figures 2 and 3. Steady-state force and moment results on the single-wedge airfoil with a sharp leading edge are given in figures 4 to 12. The effects of leading-edge bluntness on the normal-force coefficient for the single-wedge airfoil are shown in figure 13. Unsteady pressure results on the single wedge are shown in figures 14 and 15.

Figures 16 to 20 show the results obtained on the diamond-shaped profile. Comparisons of some aerodynamic characteristics of the two airfoils are presented in figures 21 to 23.

DISCUSSION

Schlieren Photographs and Pressure Distributions

Schlieren photographs of the flow about the single-wedge airfoil with the sharp leading edge are shown in figure 2 at angles of attack of 0°, 4°, and 8° and Mach number up to unity. Although no photographs are presented at supersonic speeds, few changes in the flow occurred since the bow wave of the model did not become attached. Except for the slope of the shocks, the flow configuration at $M = 1.0$ remained essentially unchanged up to the highest test Mach number.

In figure 2(a) at $\alpha = 0^\circ$, the most conspicuous flow characteristic at the lower Mach numbers is the existence of a large, clearly defined vortex system in the wake. Also noticeable at these Mach numbers are the weak pressure fronts advancing upstream over the model and produced by the shedding vortices. As the supersonic zone near the shoulder (100-percent-chord station) becomes larger with increasing stream Mach number, these pressure fronts can no longer proceed upstream and shocks appear downstream of the trailing edge. At a Mach number near 0.92 an expansion of the supersonic flow occurs at the shoulder that causes the

boundaries of the flow past the dead airspace at the base of the model to converge sharply. As a consequence of this flow change, the vortex system becomes relatively indistinct. Except for the increasing inclination angle of the shocks, few changes in the flow are observed with further increases in Mach number.

At an angle of attack of 4°, figure 2(b), the flow is separated over the upper surface at low Mach numbers and becomes attached at the leading edge at a Mach number of approximately 0.80. Separation does not occur at the foot of the normal shock on the upper surface although some turbulent flow is observed in the photographs (for example at $M = 0.85$). This turbulence arises from the flow near the side wall model juncture and is not representative of conditions existing over the entire model span.

In figure 2(c) at $\alpha = 8^\circ$, there is extensive separation on the upper surface at Mach numbers below that for leading-edge flow attachment. The vortex system observed for the blunt base at the lower angles of attack is not well formed until the flow over the upper surface becomes attached at the leading edge near $M = 0.77$. After leading-edge flow attachment has occurred, the pattern of flow changes in the wake follows that described for $\alpha = 0^\circ$.

It is significant to note that on this profile, as opposed to more conventional thick airfoils, shocks are not formed on the lower surface. The location of minimum pressure at the trailing edge positions the lower surface shock downstream of the airfoil; hence, the loading on the lower surface does not contribute to any abrupt changes in lift, pitching moment, or center-of-pressure location.

Figure 3 has been prepared to illustrate the marked improvements in chordwise loading which may be expected by locating the maximum thickness at the trailing edge. In the figure, pressure-distribution plots have been superimposed on the schlieren photographs of the single-wedge airfoil section and are compared with similar data for the diamond profile obtained from reference 3. It may be observed that, at low speeds, for both angles of attack (4° and 8°) the flow is separated on the upper surface over the afterbody of the diamond airfoil and this portion of the airfoil is carrying a negligible percentage of the total load. The entire chord of the single wedge, on the other hand, is supporting a positive load. As the Mach number is increased to about 0.90, a positive loading is still maintained over the chord of the single wedge whereas the afterbody of the diamond airfoil has developed negative load. This reversed loading results in large variations in lift and pitching moment with Mach number in the high subsonic range. Positive lift is regained over the rear part of the diamond profile at a Mach number near unity as the upper surface shock reaches the trailing edge.

Aerodynamic Data for the Single Wedge

Normal force.- The variation of section normal-force coefficient with Mach number for constant angles of attack is shown in figure 4 for the sharp-leading-edge single-wedge airfoil. Large changes in normal force occurred at the high angles of attack at Mach numbers near 0.80 as the result of the flow attachment over the upper surface shown previously in figure 2. A study of schlieren motion pictures indicated that the attachment probably occurs over a shorter interval of Mach number than indicated by the fairing through the data at angles of attack of 6° and 8° in figure 4. A diminution of normal force with increasing Mach numbers was characteristic at the higher angles of attack for all test Mach numbers above those for leading-edge attachment. The variation of section normal-force coefficient with angle of attack at constant Mach numbers is shown in figure 5. (In order to facilitate presentation of the data, staggered scales have been used in a few of the figures and care should be taken in identifying the zero axis for each curve.) The slopes of these curves, obtained at two normal-force coefficients, are presented in figure 6. The data of this figure indicate that large normal-force-curve slopes are maintained throughout the speed range at moderate ($c_n = 0.4$) normal-force coefficients. At $c_n = 0.4$ the single-wedge airfoil exhibited normal-force-curve slopes considerably in excess of those obtained in reference 10 for the NACA 65A006 airfoil. The large normal-force-curve slopes obtained at $c_n = 0.8$ and at Mach numbers less than 0.85 are not maintained throughout the Mach number range.

Pitching moment and center-of-pressure travel.- The section pitching-moment coefficients about the leading edge as affected by Mach number are shown in figure 7 and exhibit the same general characteristics as the normal-force data. The data of figure 7 have been crossplotted in figure 8 to indicate the effect of section normal force on section pitching moment at constant Mach numbers. Moment irregularities generally exhibited by thick airfoils do not occur on this profile at the high subsonic Mach numbers. This result is not unexpected since the cause of large moment changes, that is, negative loading on the rear portion of the profile, has been eliminated to a great extent by the absence of shocks on the lower surface.

Center-of-pressure location as affected by Mach number is shown in figure 9. The large loading at the trailing edge causes the center of pressure for the single-wedge airfoil to be somewhat more rearward at the lower speeds than for a conventional thick airfoil. Exceptionally gradual movement of the center of pressure is exhibited at all section normal-force coefficients. Over the Mach number interval between the highest test Mach number and that for bow wave attachment, it is expected that the center of pressure will move toward the 50-percent-chord location predicted by supersonic theory.

Drag.- The pressure drag results for this profile have been separated into forebody, base, and total-pressure drag coefficients and are presented in figure 10.

Section forebody drag coefficients, figure 10(a), exhibit a continuous increase through sonic velocity and up through the highest test Mach numbers. The negative forebody drag coefficients shown for the low angles of attack below Mach numbers of 0.80 are the result of negative pressures existing over most of the model surfaces.

Base-pressure results are shown in figure 10(b). The base pressure coefficients generally become more negative for all angles of attack as the Mach number approaches unity. At supersonic velocities the coefficients increase with Mach number at approximately the same rate as the coefficient for a vacuum. At low speeds and angles of attack near zero lift, the base pressure gradually diminishes until a Mach number of about 0.87 is reached. At this Mach number, the schlieren photographs (fig. 2(a)) indicate that the boundaries of the dead-air region are beginning to collapse and a more rapid decrease in pressure is observed.

Leading-edge separation at the higher angles of attack and at low speeds causes significant increases in base pressure coefficients (fig. 10(b)) as compared with those measured at zero lift. The schlieren photographs at $\alpha = 8^{\circ}$, figure 2(c), show that the vortex street in the wake is not well formed until leading-edge flow attachment has occurred. After attachment, the pumping action of the wake is confined to the base area and, consequently, there is a rapid reduction in base pressure.

As the terminal shock on the upper surface passes onto the boundary layer emerging from the shoulder of the model, the high pressures behind the shock are transmitted into the base region. This phenomenon is particularly noticeable at $\alpha = 6^{\circ}$ and $M = 0.83$ as a reversal of the normal trend of decreasing base pressure.

Total-pressure-drag results are presented in figure 10(c). As expected from the variations of base pressure with Mach number, the maximum drag coefficients are reached at Mach numbers near 1.0. Above sonic velocity there is a continuous decrease in drag coefficient. It is anticipated that when the bow wave becomes attached to the leading edge there will be additional reductions in the drag coefficients but these are expected to be small percentagewise due to the predominance of base drag.

Section forebody and total drag coefficients as a function of section normal-force coefficients are shown in figure 11. Since it is known that base drag may be substantially reduced by utilizing base bleed, forebody drag represents a minimum drag condition and is included in this figure. At normal-force coefficients up to about 0.50, the total drag shows little change with normal force for all Mach numbers. At subsonic

speeds there is little drag increase due to further increases in normal force and at the higher lift conditions there are significant reductions. These reductions at Mach numbers less than 0.90 are the result of the decrease in base drag with angle of attack noted previously in figure 10(b).

Normal-force—drag ratios for forebody and total drags are shown in figure 12 plotted against section normal-force coefficient for various constant Mach numbers. In figure 12(a) it is observed that the first peak n/d_f diminishes with increases in Mach number and compares favorably with maximum normal-force—drag ratios obtained on thin airfoils (ref. 10). With further increases in normal-force coefficient beyond $c_n = 1.0$, the values of n/d_f continue to increase, the increase being less at the higher Mach numbers.

Of greater practical interest is the variation of normal-force—total-drag ratios shown in figure 12(b). Because of the subsonic reduction in base drag with increasing angle of attack, the maximum value of n/d_t would not be obtained until some extreme angles of attack were reached.

Effects of changes in leading-edge radius.- Changes in leading-edge radius from 0 to 1 percent chord generally had minor effects on the forces and no overall improvements could be observed (fig. 13). Pressure drag results were not obtained on the rounded leading-edge profiles because of the uncertainty of fairing the pressure distributions in the leading-edge region. It is anticipated, however, that there will be some reduction in drag due to the large suction pressures existing over the rounded leading edge. Moments and center-of-pressure locations were essentially unaffected by increasing the leading-edge radius.

Pressure Pulsations

Unsteady pressures on the single-wedge airfoil, measured at several chordwise stations and on the base, are shown in figures 14 and 15 at Mach numbers up to unity. The double-amplitude pressure pulsations are expressed in terms of the free-stream dynamic pressure and were obtained in the same manner as described in reference 12.

At an angle of attack of 0° the pressure fluctuations are small. (See fig. 14.) There is some indication that the pressures immediately upstream of the shoulder are slightly affected by the strong vortex in the wake, but the influence diminishes as the stream Mach number increases and the supersonic zone existing there becomes larger. Changes in leading-edge radius have minor effects on the unsteady pressures at this angle of attack. The amplitudes of the pressure pulsations have increased somewhat at $\alpha = 4^\circ$, particularly near the leading edge. No definite

trend exists in the data as regards changes in leading-edge radius, and the significance of the high pulsations near the leading edge with a leading-edge radius of 0.5 percent chord is not known. Further increases in angle of attack produce higher values of $\Delta p/q$ and the influence of leading-edge radius becomes more pronounced. Pressure pulsations measured on the profile with a 1-percent-chord leading-edge radius at $\alpha = 8^\circ$ are significantly higher than for the smaller leading-edge radii. For each leading-edge condition there is a marked reduction in the level of pulsations as leading-edge flow attachment occurs.

Also shown in figure 14 are the data for the NACA 65A006 airfoil obtained from reference 12. It is observed that the maximum values of $\Delta p/q$ occurring over the chord of this airfoil become significantly higher with increased angle of attack than those measured on the single-wedge profile. Maximum pressure pulsations measured on the upper surface of the wedge airfoil generally remained below 14 percent of the dynamic pressure; this value is a criterion established in reference 12 as a rough limit for possible buffeting.

Figure 15 shows the values of pressure pulsations measured at the 96-percent-chord station together with those measured on the base of the model. Pressure pulsations over the base at zero lift average about 15 percent of the dynamic pressure for all Mach numbers below that for which the wake collapses. Pressures at the 96-percent-chord station are influenced to some extent at low speeds by oscillations in the wake but the pulsations diminish slightly with increasing Mach numbers. Changes in leading-edge radius have little effect on the base pressure oscillations or those measured at the 96-percent-chord station at nonlifting conditions.

Base pressure pulsations at $\alpha = 4^\circ$ were generally lower than those at zero lift. The amplitudes of the pulsations on the upper surface at the 96-percent-chord station were about equal to those measured at a similar location on the lower surface. This result would be expected since the schlieren photographs (fig. 2(b)) indicated no separation at the foot of the normal shock on the upper surface. Increases in leading-edge radius bring about minor reductions in the level of base pressure pulsations but, in general, do not influence the pressure oscillations at the 96-percent-chord station to a perceptible extent.

At an angle of attack of 8°, at low speeds, the flow is separated from the leading edge on the upper surface and the base pressure pulsations are low, being comparable to those measured over the upper surface. The schlieren flow photographs (fig. 2(c)) indicate that the upper surface and the base are submerged in the wake, and it would be expected that the pulsations on these surfaces would have generally the same magnitude. As the Mach number increases and leading-edge flow attachment occurs, the vortex system in the wake becomes well defined causing the

base pressure pulsations to approach their maximum amplitudes. Pressure pulsations at the 96-percent-chord station on the upper surface have maximum amplitudes at Mach numbers near that for leading-edge flow attachment and diminish somewhat as the normal shock passes downstream of the trailing edge. Increasing the leading-edge radius at $\alpha = 8^{\circ}$ generally raises the amplitude of the pulsations over the rear part of the model. The lower surface pulsations, however, are only slightly affected by changes in angle of attack or leading-edge radius.

Aerodynamic Data for the Diamond Shaped Airfoil

Section normal-force, drag, and leading-edge pitching-moment coefficients for the diamond profile are shown in figure 16. The Reynolds number range for this profile varied from 2.4×10^6 to 2.8×10^6 based on the 4-inch chord and represents values considerably in excess of those reported for previous investigations of similar profiles. (See refs. 3, 4, and 6.) It is not unexpected, therefore, that previously published results show some quantitative disagreement with the present data; the difference being attributable, in large part, to changes in Reynolds number.

Normal force.- The significant changes in normal force at subsonic Mach numbers are due to leading-edge flow attachment and load reversals on the afterbody of the profile shown previously in figure 3. Abrupt increases in normal force at Mach numbers near 0.80, at angles of attack of 6° and 8°, are the results of flow attachment over the forebody near the leading edge. An examination of the pressure distributions at these angles of attack and Mach numbers indicated that the greatest part of the total normal force was carried by the forebody and that the afterbody, due to extensive separation, carries only a small part of the total load. Comparisons of the single-wedge pressure distributions with the pressure distributions over the forebody of the diamond profile show marked similarities (fig. 3). Minor differences do occur but are confined to the region near the shoulder. The comparisons of figure 3 give strong evidence that the flow over the forebody of the diamond airfoil is essentially represented by the flows over the single wedge.

As was observed in figure 3, the large losses in normal force encountered by the diamond airfoil at Mach numbers between 0.80 and 1.0 are due to the development of negative loads on the afterbody. Schlieren motion pictures indicate that, after supersonic flow is established at the shoulder, the shocks on both upper and lower surfaces simultaneously move rearward to about the 60-percent-chord station. As the Mach number continues to increase the lower-surface shock continues its rearward movement to the trailing edge. Minimum normal force occurs when this lower-surface shock arrives at the trailing edge. Further increases in speed cause the upper-surface shock to begin its rearward movement from

the 60-percent-chord location. Normal force is again recovered near Mach number 1.0 as this shock reaches the trailing edge.

Drag.- At the lower subsonic speeds, large increases in drag are observed to occur with increasing angle of attack and are due to extensive separation over the upper surface. At lifting conditions, a rapid rise in drag is exhibited at Mach numbers greater than 0.90 and is the result of the establishment of supersonic flow over the upper surface of the profile afterbody. Maximum drag coefficients occur as the shock, which terminates this low-pressure region, reaches the trailing edge. Increases in Mach number thereafter bring about reductions in drag coefficient for all angles of attack.

An illustration of the severe drag penalties incurred by removing the afterbody of a profile is obtained by comparison of the data of figure 10(c) for the single-wedge airfoil with the data of figure 16 for the diamond airfoil. At sonic velocity, for example, the zero-lift drag of the single wedge is about 2.75 times the drag of the diamond section of equivalent leading-edge angle and frontal area.

Pitching-moment coefficient.- The effect of Mach number and angle of attack on the pitching-moment coefficients about the leading edge is also shown in figure 16. As previously mentioned, the severe moment reversals exhibited by this profile are a consequence of the load reversals over the afterbody at high subsonic speeds. The data indicate that flow attachment has a negligible effect on the leading-edge moments since the change in loading occurs near the moment axis and does not introduce an opposing couple.

Effect of normal force on drag.- The effects of normal force on the drag at constant Mach numbers are shown in figure 17. Subsonic results (fig. 17(a)) are in qualitative agreement with those of reference 3. Supersonic results (fig. 17(b)) show relatively small changes in drag due to variations in Mach number, particularly at the higher lift conditions. The influence of Mach numbers and normal force on the aerodynamic efficiency of the diamond airfoil is shown in figure 18. Maximum normal-force—drag ratios obtained from this figure are shown as a function of Mach number in figure 19. It is observed that maximum normal-force—drag ratios diminish throughout the subsonic range of the tests. Agreement with second-order supersonic theory, shown in the figure, is exceptionally close but can be considered fortuitous since neither normal force nor drag results are comparable to values computed from theory at low supersonic velocities where the bow wave is detached. The present results on a diamond profile, along with those of reference 10 on conventional NACA airfoils, indicate that maximum normal-force—drag ratios may be estimated with good accuracy in the low supersonic Mach number range even though the bow shock is detached and regions of subsonic flow exist over the surfaces of the airfoil.

Pitching-moment variation with normal force and some comparisons of the data for the two airfoils.- Changes in leading-edge pitching-moment coefficient as affected by normal-force coefficient are shown in figure 20. The slopes of these curves, determined at $c_n = 0.3$, are presented in figure 21. Also shown in figure 21 are the results obtained on the single-wedge airfoil section. The undesirable pitching-moment behavior exhibited by the diamond airfoil has generally precluded its use as an aerodynamic surface in the transonic range. Gradual changes in $dc_{m,le}/dc_n$ for the single-wedge airfoil section occur over the speed range except for the short interval in Mach number below 1.0.

Further comparisons of the data obtained on the two profiles are presented in figure 22 where the Mach number effects on center-of-pressure location are shown for two section normal-force coefficients. In contrast to the single-wedge airfoil, the diamond airfoil exhibits large forward movements of the center of pressure in the Mach number interval from 0.80 to 1.0 because of the adverse loadings at the trailing edge.

The lift effectiveness of both airfoils is compared in figure 23, wherein it is seen that the single-wedge airfoil maintains a significantly higher normal-force-curve slope throughout the speed range. The loss in normal-force-curve slope at supersonic speeds is not as severe for the diamond airfoil as for the single-wedge airfoil, however. It is of interest to note that the results for the double-wedge airfoil are in agreement with the theoretical results of reference 13 at sonic velocity even though the experimental slopes were obtained at $c_n = 0.4$, a section normal-force coefficient considered beyond the scope of small-disturbance theory.

CONCLUDING REMARKS

An investigation has been conducted at transonic speeds of the two-dimensional aerodynamic characteristics of a single-wedge airfoil section of 20-percent thickness and a symmetrical double-wedge or diamond section having the same leading-edge included angle. The results reveal that, except for drag, the single-wedge profile is aerodynamically superior to the diamond profile. The single-wedge airfoil section exhibited normal-force-curve slopes considerably in excess of those obtained previously on conventional thin airfoils. Pitching-moment irregularities and erratic center-of-pressure movements characteristic of thick airfoil sections in this Mach number range were not observed on the single wedge.

Pressure pulsations measured over the upper surface of the wedge generally remained low. The effect of angle of attack on the amplitudes of these pulsations was considerably less than that obtained on an

NACA 65A006 airfoil. Base pressure pulsations averaged about 15 percent of the free-stream dynamic pressure and were substantially reduced upon the collapse of the boundaries enclosing the dead airspace at the base of the model as the Mach number increased beyond 0.92. Rounding the leading edge of the profile did not effect significant improvements of the steady-state forces and, in general, increased the amplitudes of the unsteady pressure pulsations.

Langley Research Center,
National Aeronautics and Space Administration,
Langley Field, Va., February 9, 1959.

REFERENCES

1. McLellan, Charles H.: A Method for Increasing the Effectiveness of Stabilizing Surfaces at High Supersonic Mach Numbers. NACA RM L54F21, 1954.

2. Lindsey, W. F., Daley, Bernard N., and Humphreys, Milton D.: The Flow and Force Characteristics of Supersonic Airfoils at High Subsonic Speeds. NACA TN 1211, 1947.

3. Humphreys, Milton D.: An Investigation of a Lifting 10-Percent-Thick Symmetrical Double-Wedge Airfoil at Mach Numbers up to 1. NACA TN 3306, 1954.

4. Bartlett, G. E., and Peterson, J. W.: Wind-Tunnel Investigation of Double-Wedge Airfoil at Subsonic Speeds. Bumblebee Rep. No. 53 (Contract NOrd-8993), Cornell Aero. Lab., Aug. 1946.

5. Vincenti, Walter G., and Wagoner, Cleo B.: Transonic Flow Past a Wedge Profile With Detached Bow Wave. NACA Rep. 1095, 1952. (Supersedes NACA TN's 2339 and 2588.)

6. Vincenti, Walter G., Dugan, Duane W., and Phelps, E. Ray: An Experimental Study of the Lift and Pressure Distribution on a Double-Wedge Profile at Mach Numbers Near Shock Attachment. NACA TN 3225, 1954.

7. Bryson, Arthur Earl, Jr.: An Experimental Investigation of Transonic Flow Past Two-Dimensional Wedge and Circular-Arc Sections Using a Mach-Zehnder Interferometer. NACA Rep. 1094, 1952. (Supersedes NACA TN 2560.)

8. Eggers, A. J., Jr.: Aerodynamic Characteristics at Subcritical and Supercritical Mach Numbers of Two Airfoil Sections Having Sharp Leading Edges and Extreme Rearward Positions of Maximum Thickness. NACA RM A7C10, 1947.

9. Willmarth, William W.: The Lift of Thin Airfoils at High Subsonic Speeds. OSR TN 54-168 (Contract AF-18(600)-383), GALCIT, June 1954.

10. Ladson, Charles L.: Two-Dimensional Airfoil Characteristics of Four NACA 6A-Series Airfoils at Transonic Mach Numbers up to 1.25. NACA RM L57F05, 1957.

11. Daley, Bernard N., and Dick, Richard S.: Effect of Thickness, Camber, and Thickness Distribution on Airfoil Characteristics at Mach Numbers up to 1.0. NACA TN 3607, 1956. (Supersedes NACA RM L52G31a.)

12. Humphreys, Milton D.: Pressure Pulsations on Rigid Airfoils at Transonic Speeds. NACA RM L51I12, 1951.

13. Guderley, Gottfried, and Yoshihara, Hideo: Two-Dimensional Unsymmetrical Flow Patterns at Mach Number 1. Jour. Aero. Sci., vol. 20, no. 11, Nov. 1953, pp. 757-768.

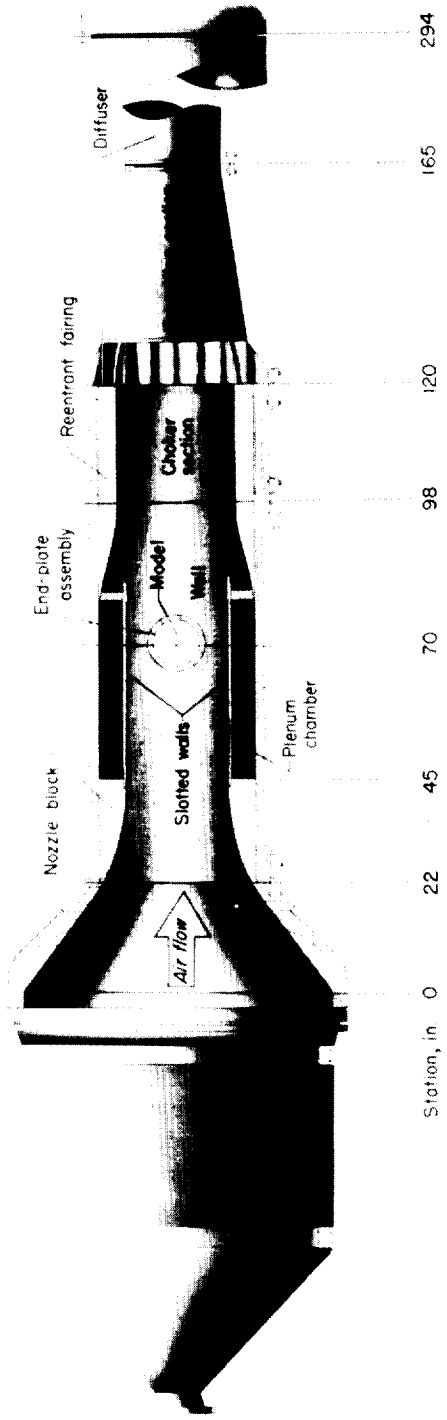

(a) General view. L-57-599

Figure 1.- Langley airfoil test apparatus.

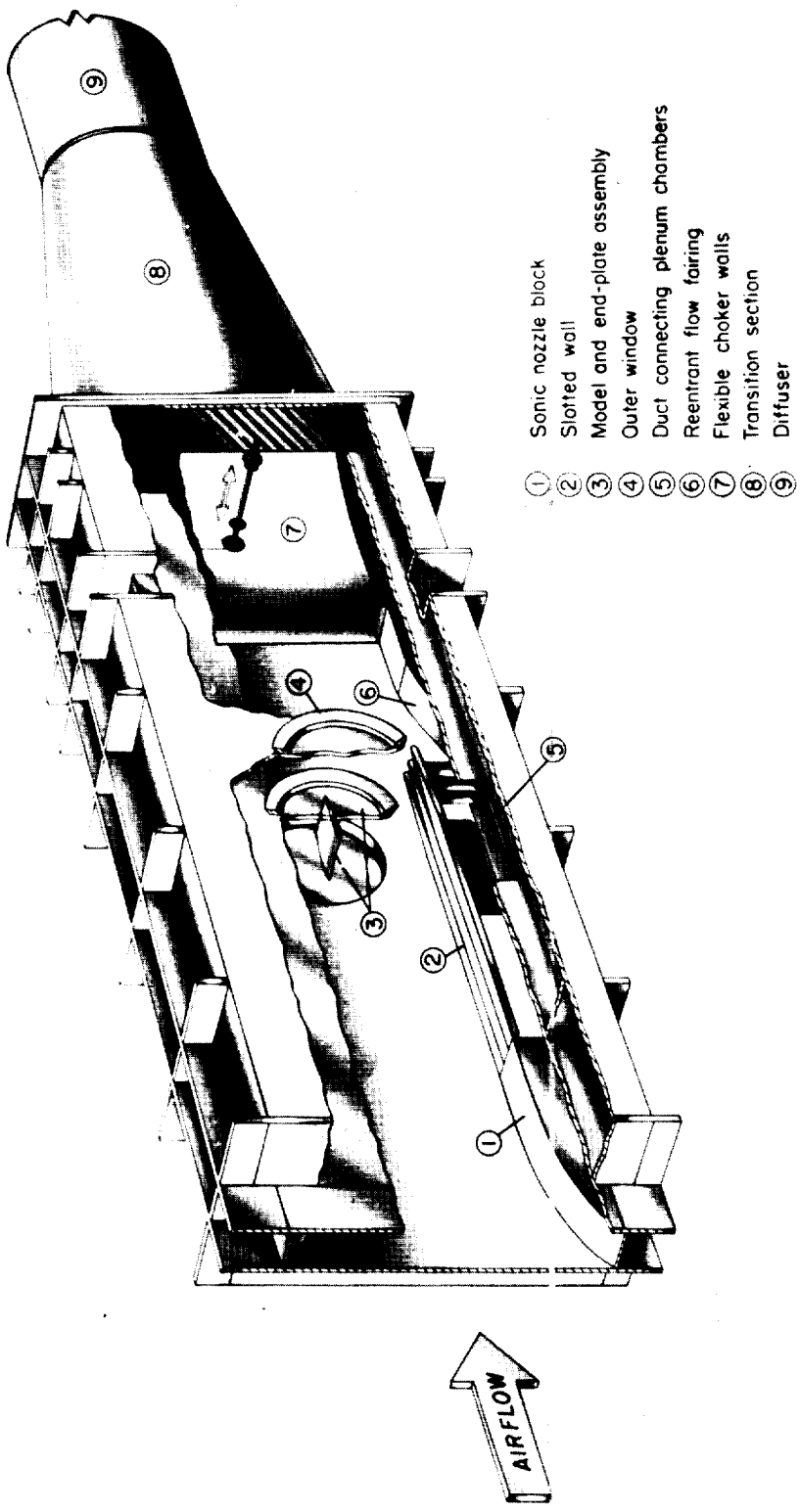

(b) Test section. L-57-598

Figure 1.- Concluded.

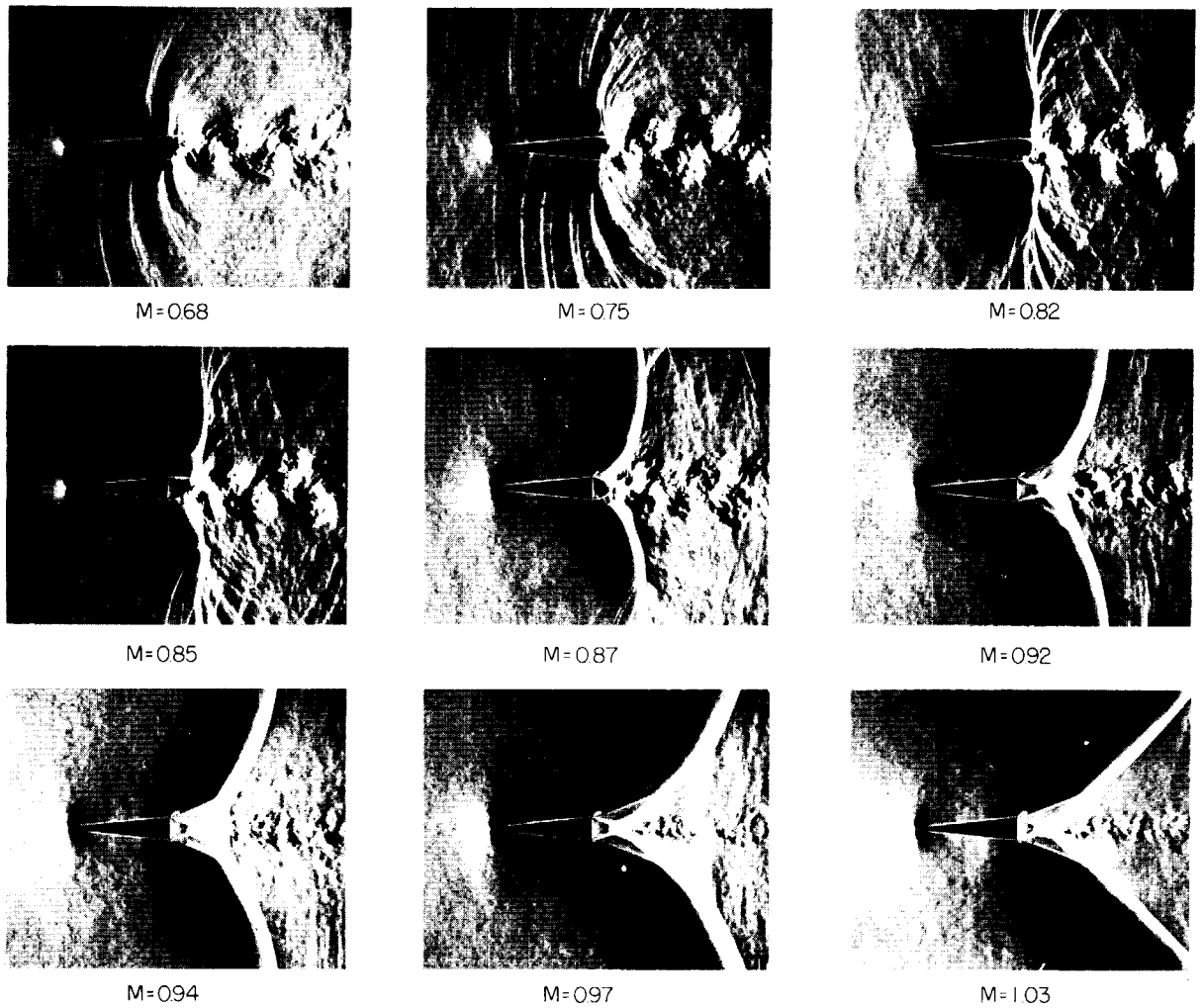

(a) $\alpha = 0^{\circ}$.

L-59-190

Figure 2.- Schlieren photographs of the flow about the single-wedge airfoil.

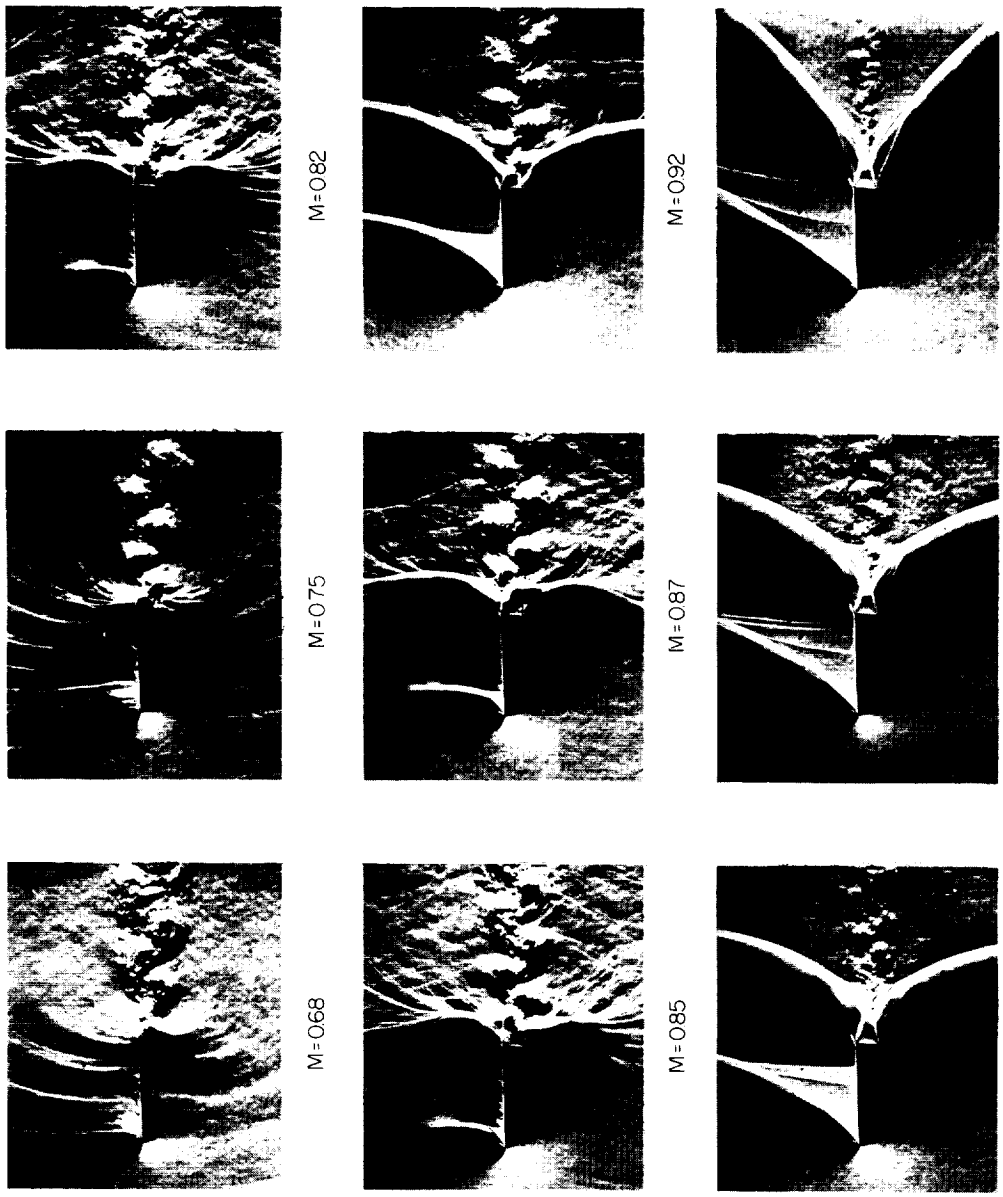

(b) $\alpha = 4^{\circ}$.

Figure 2.- Continued.

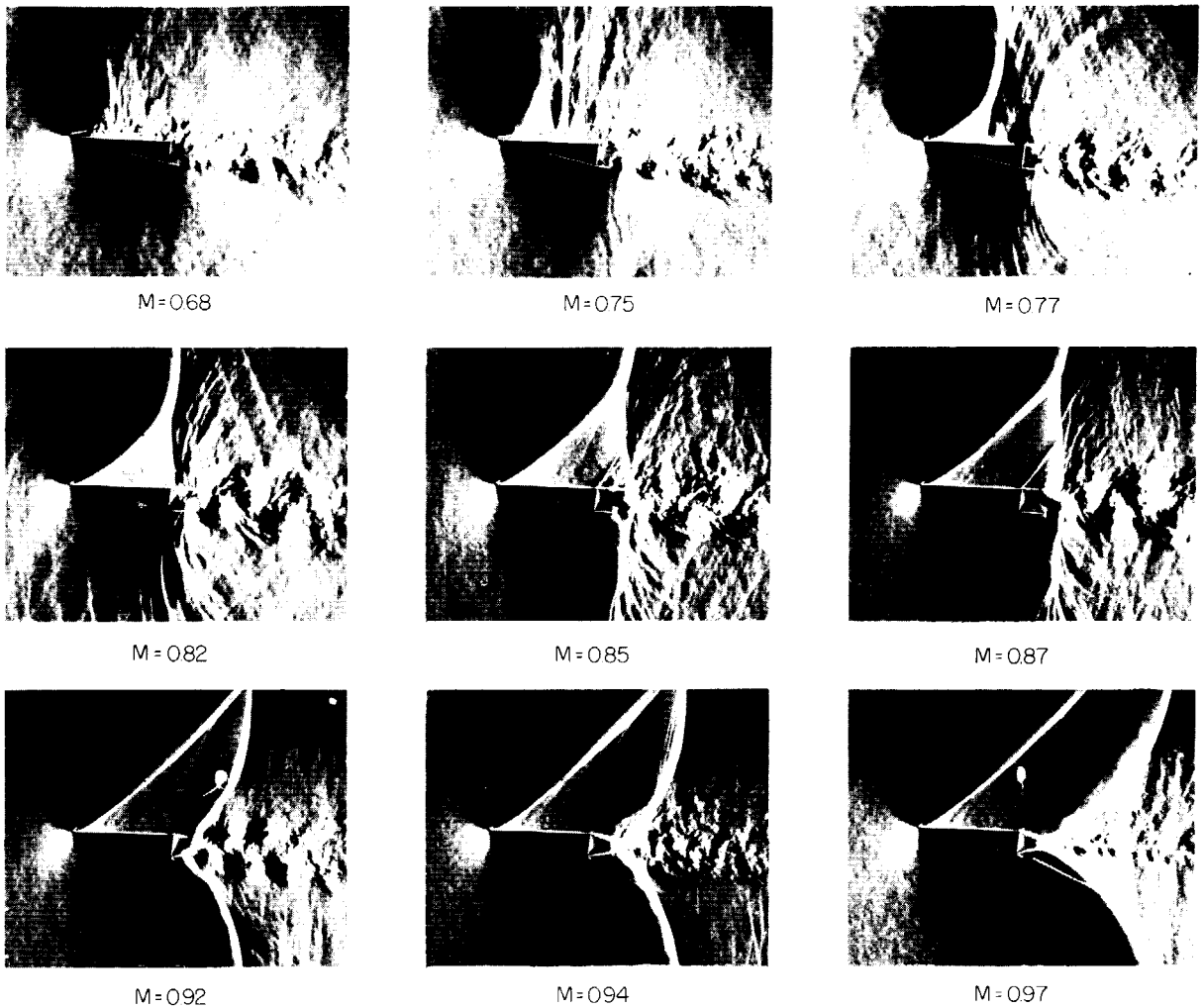

(c) $\alpha = 8^{\circ}$. L-59-192

Figure 2.- Concluded.

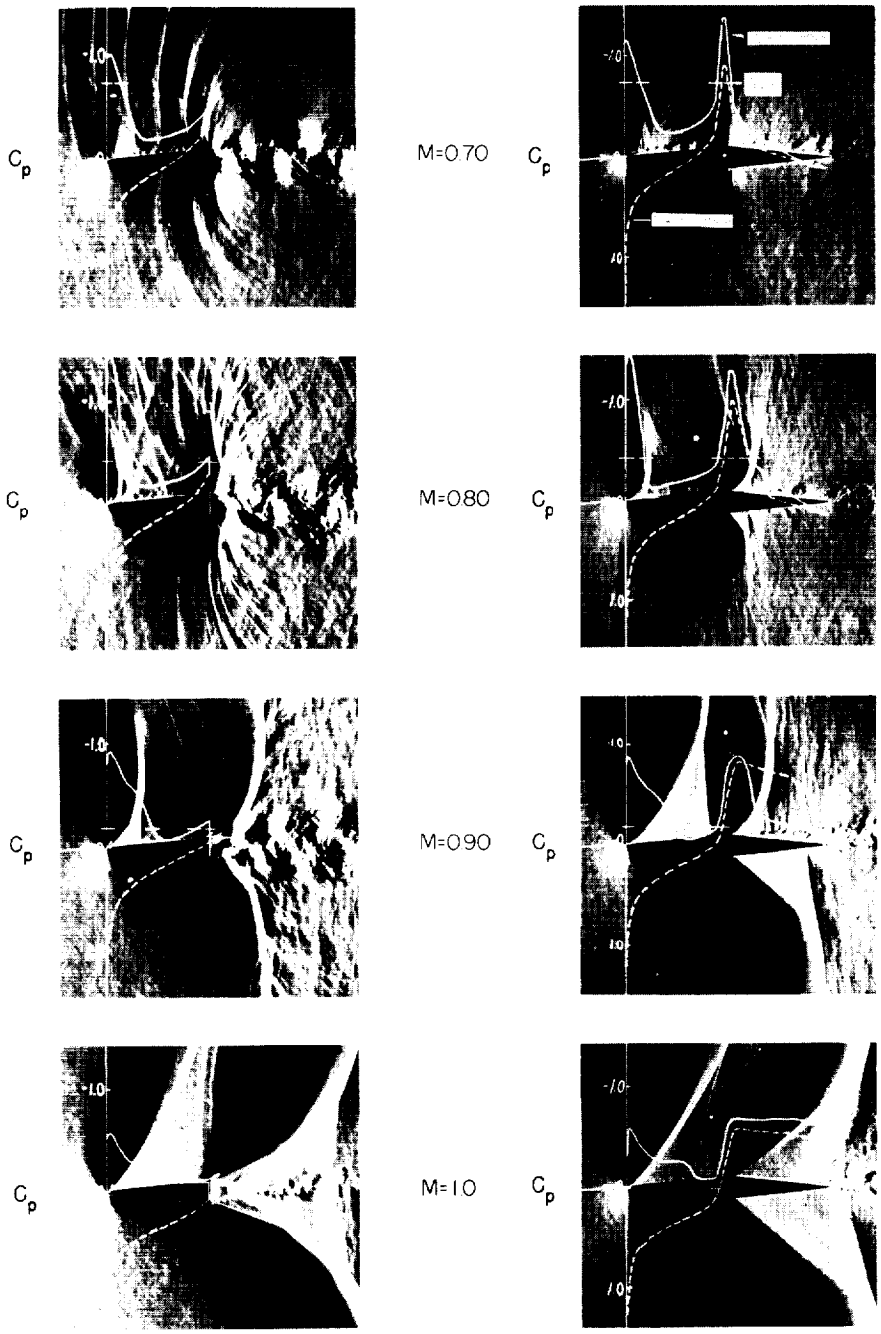

(a) $\alpha = 4^{\circ}$.

L-59-193

Figure 3.- Flow over the sharp-leading-edge single-wedge and the diamond airfoils with superimposed pressure distributions.

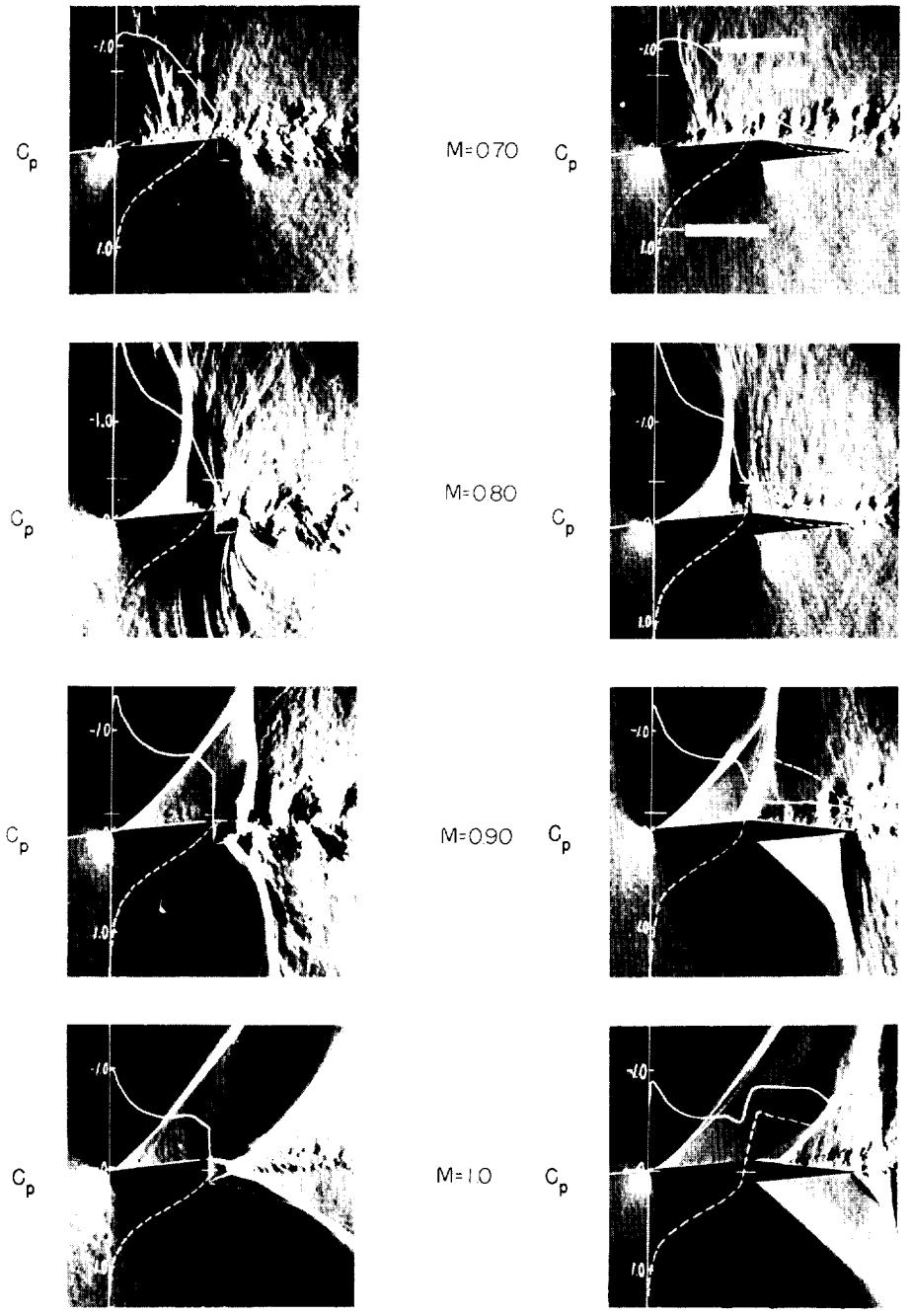

(b) $\alpha = 8^{\circ}$. L-59-194

Figure 3.- Concluded.

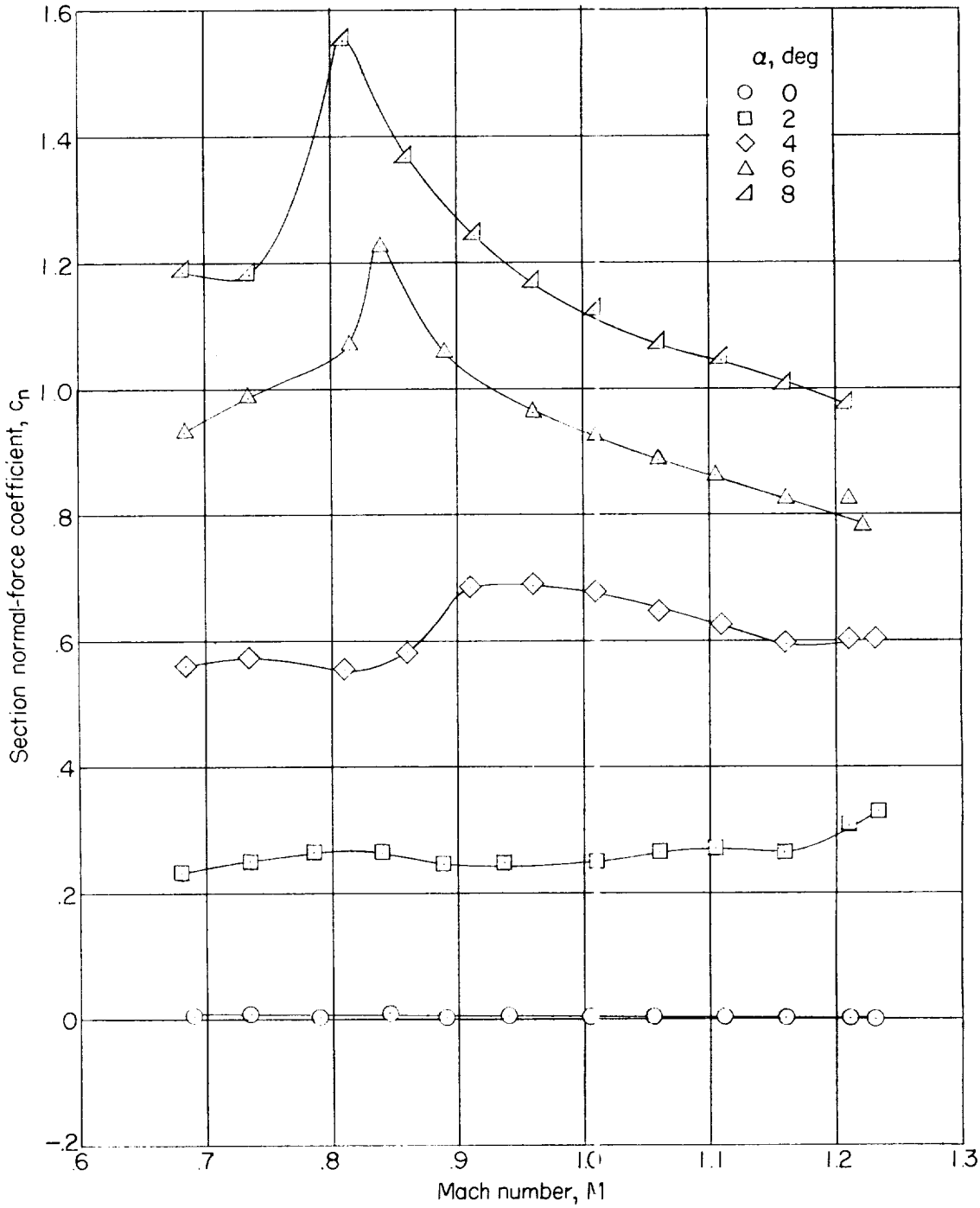

Figure 4.- Variation of section normal-force coefficient with Mach number for the sharp-leading-edge single-wedge airfoil.

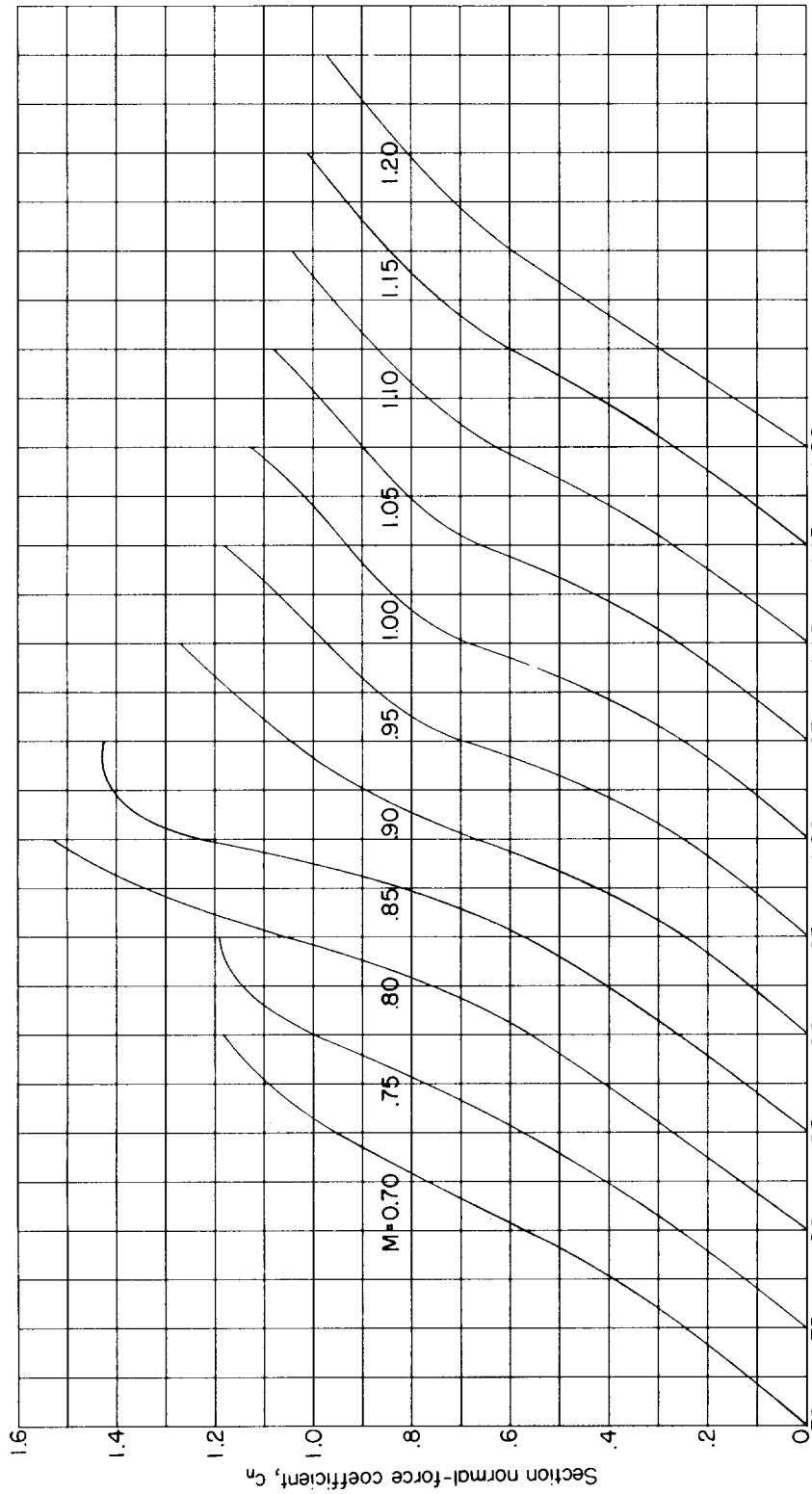

Figure 5.- Variation of section normal-force coefficient with angle of attack for the sharp-leading-edge single-wedge airfoil.

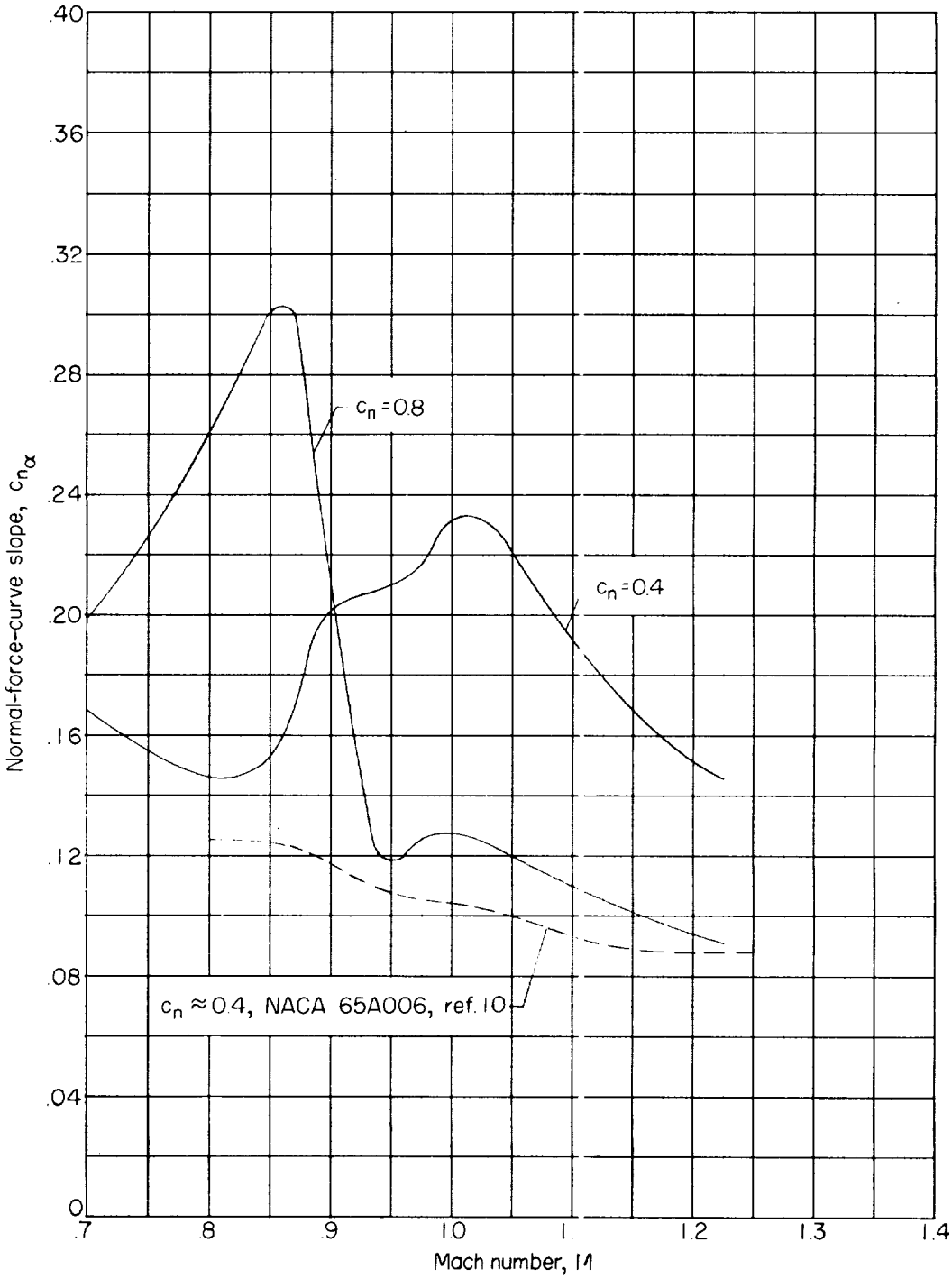

Figure 6.- Variation of section normal-force-curve slope with Mach number for the sharp-leading-edge single-wedge airfoil.

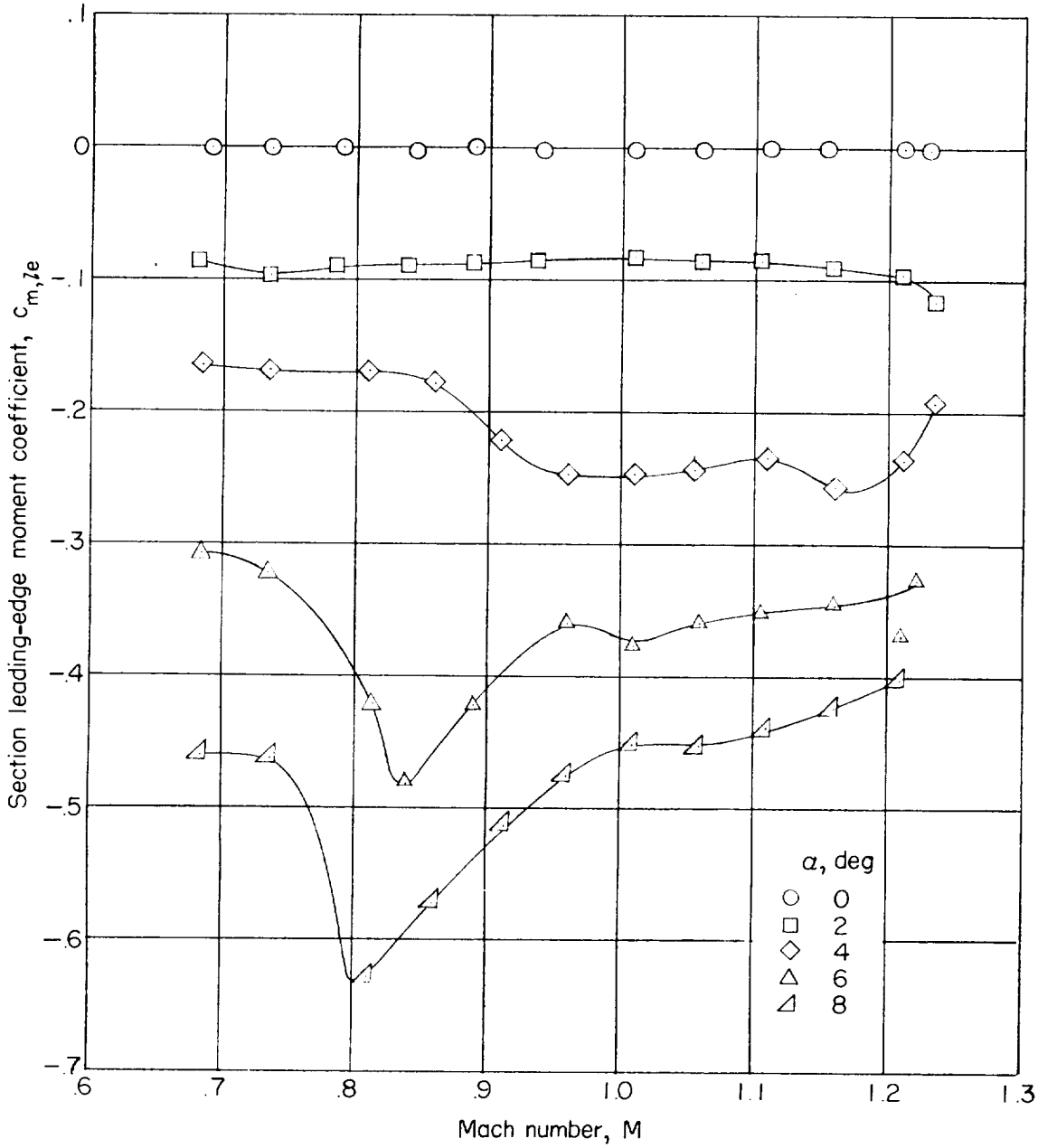

Figure 7.- Variation of section pitching-moment coefficient about leading edge with Mach number for the sharp-leading-edge single-wedge airfoil.

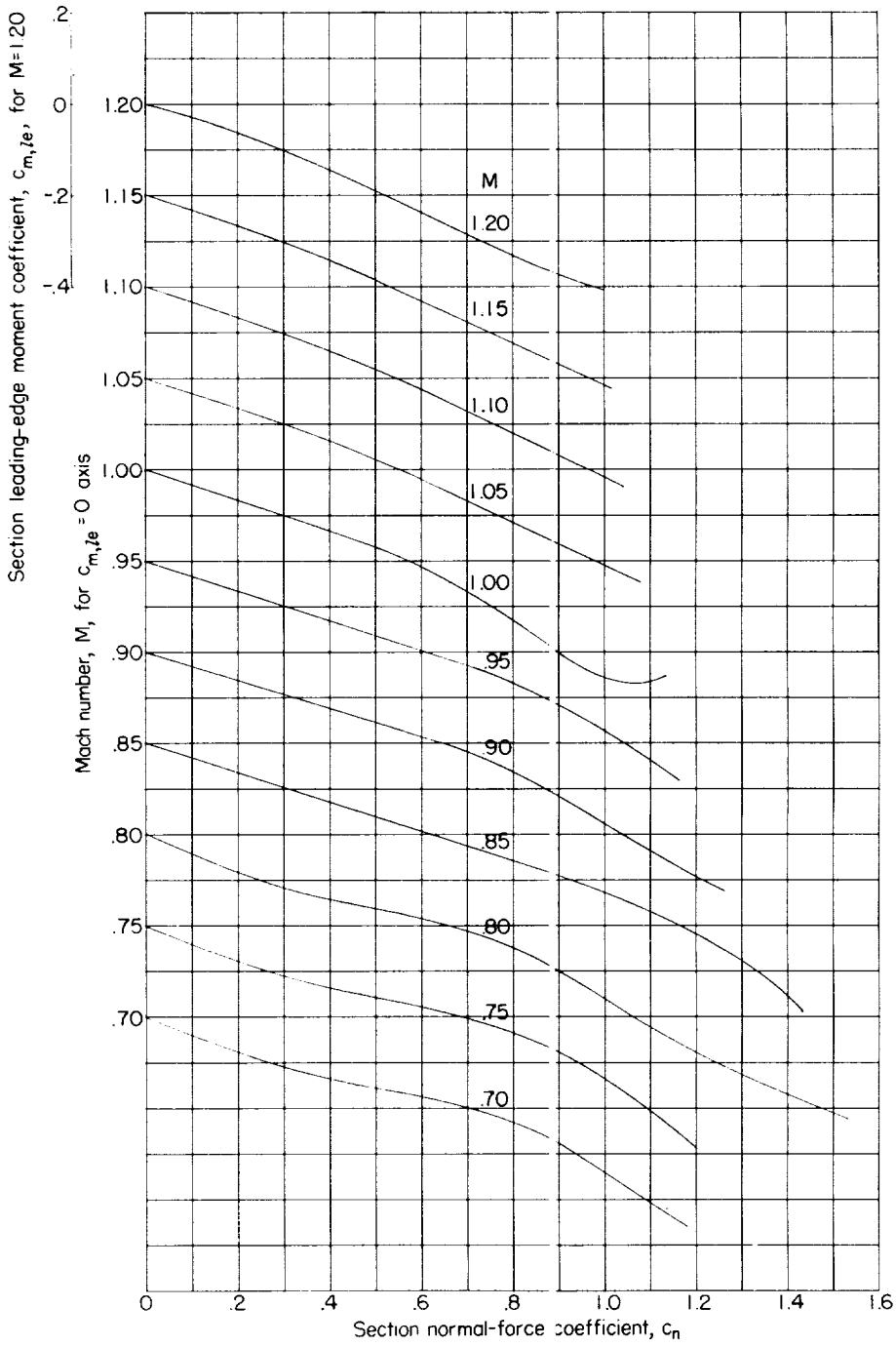

Figure 8.- Variation of section pitching-moment coefficient about leading edge with section normal-force coefficient at various Mach numbers for the sharp-leading-edge single-wedge airfoil.

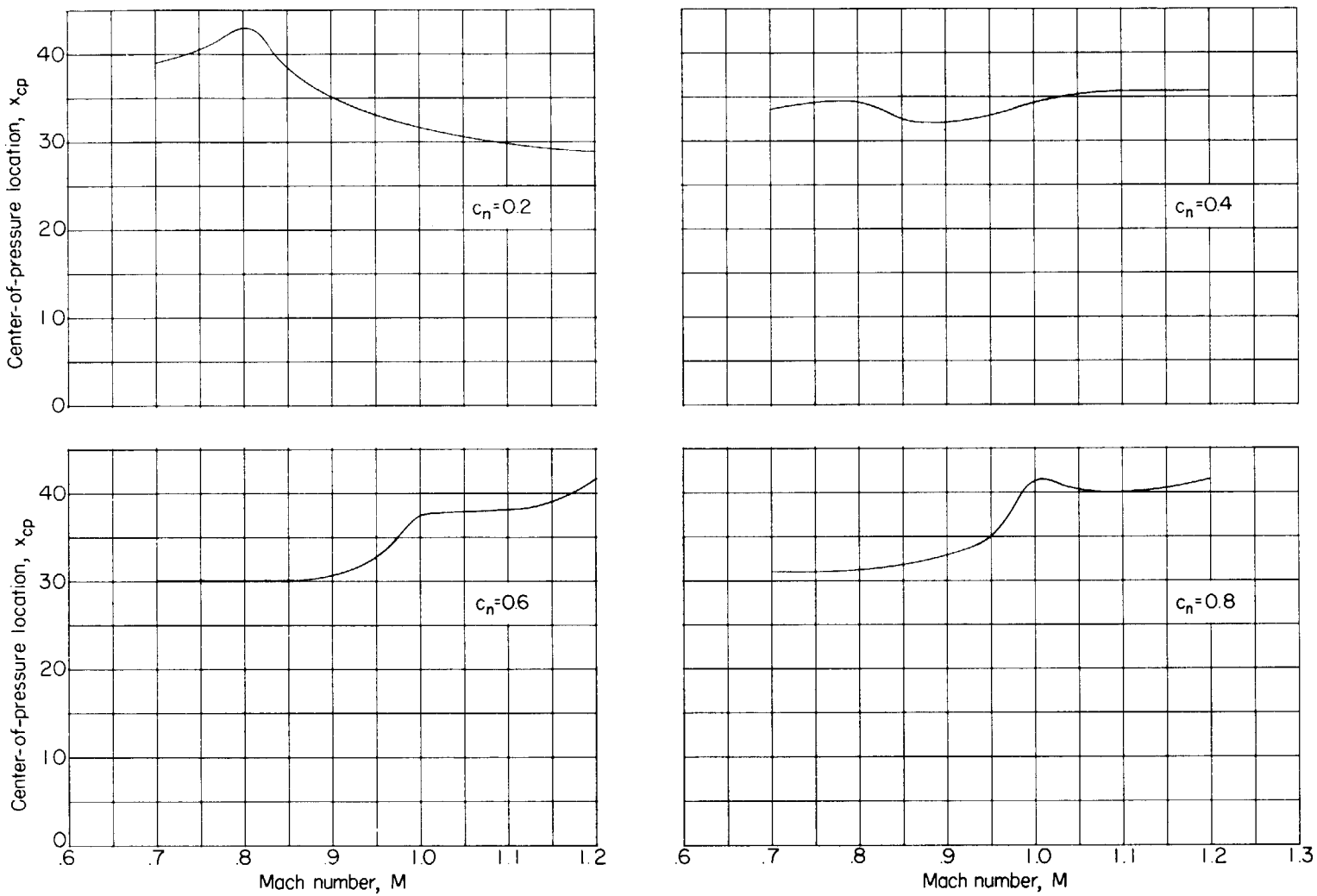

Figure 9.- Variation in chordwise location of center of pressure with Mach number for several section normal-force coefficients for the sharp-leading-edge single-wedge airfoil.

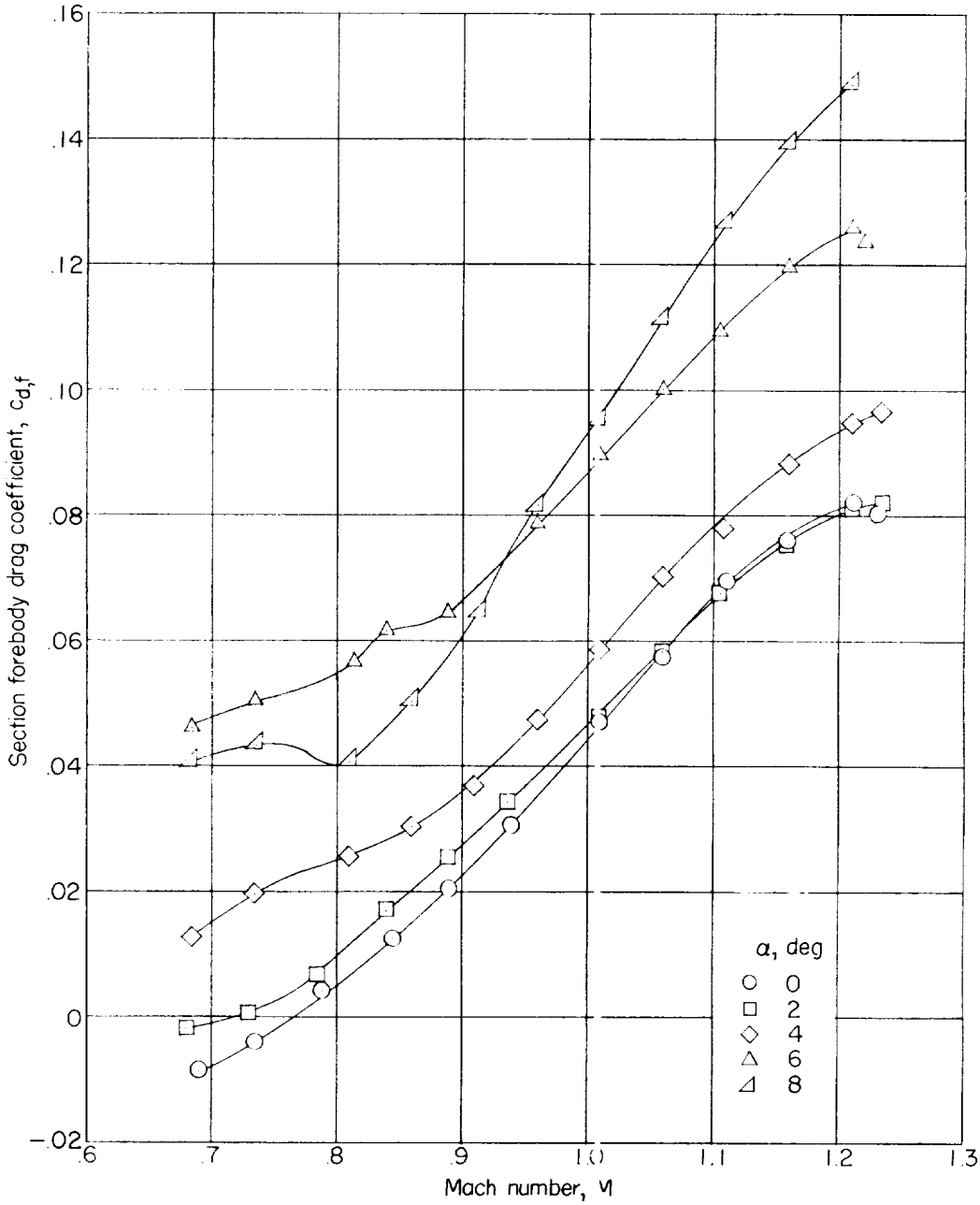

(a) Section forebody drag coefficient.

Figure 10.- Pressure drag results for the sharp-leading-edge single-wedge airfoil.

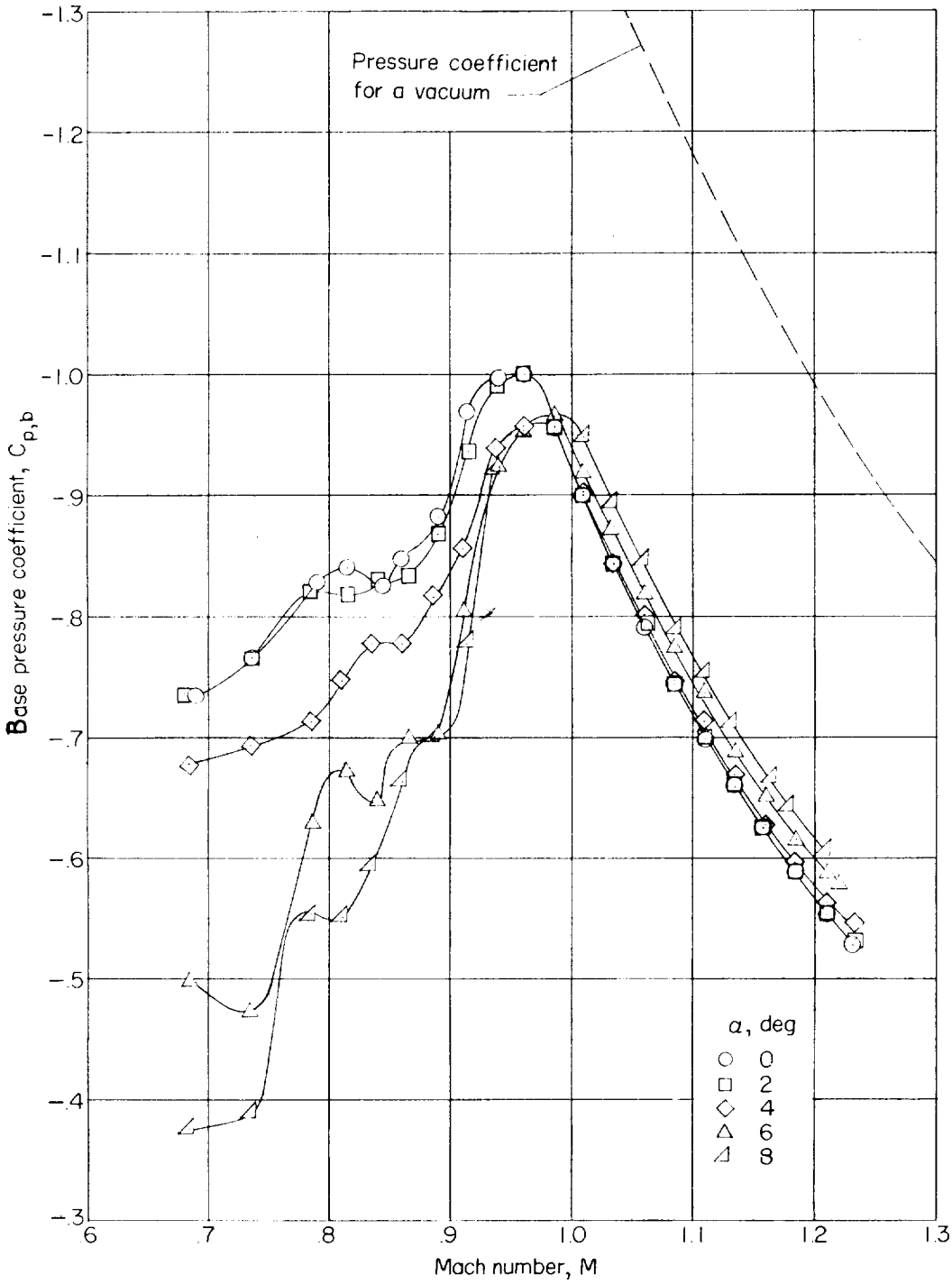

(b) Base pressure coefficient.

Figure 10.- Continued.

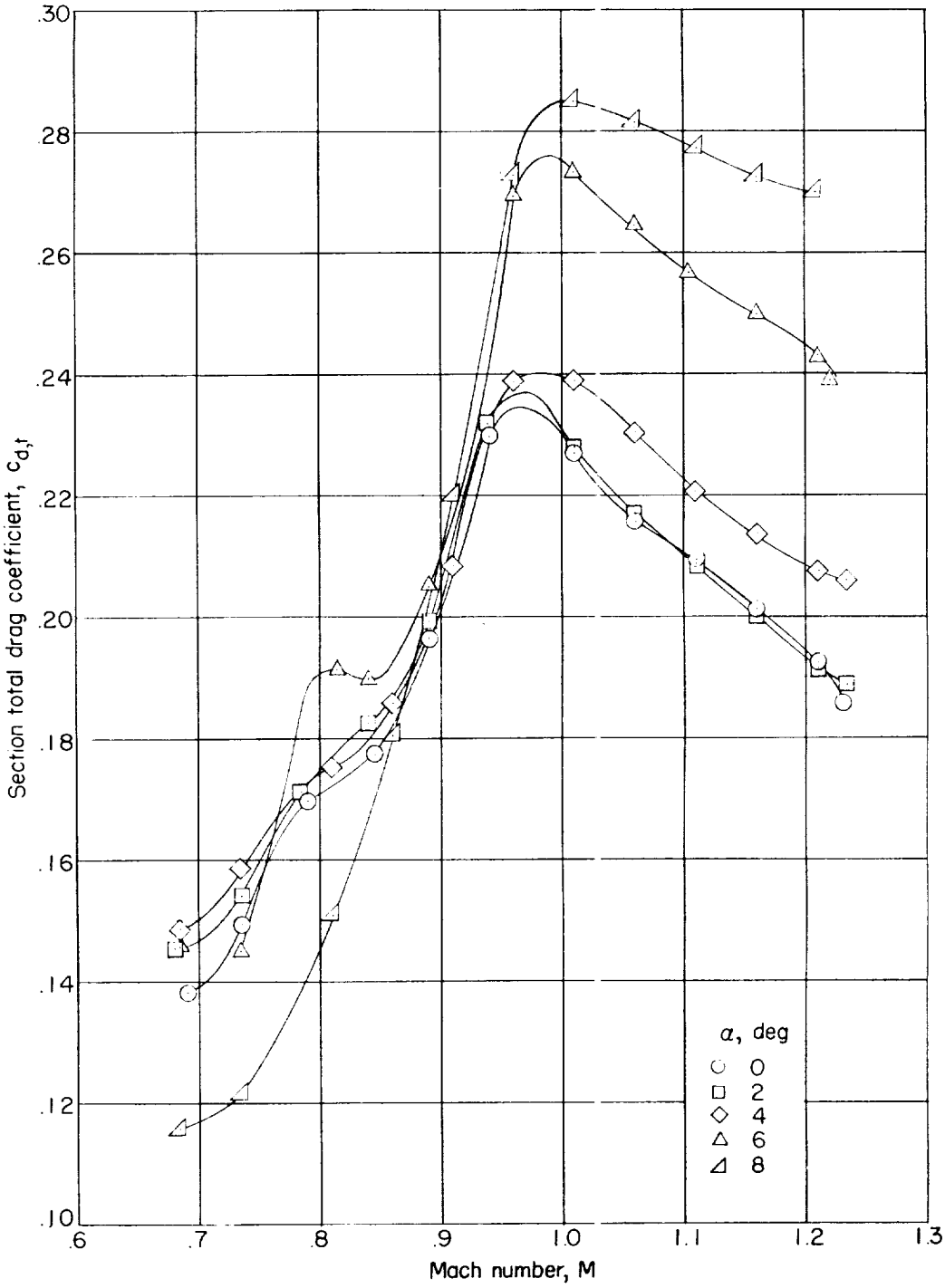

(c) Total-pressure drag coefficient.

Figure 10.- Concluded.

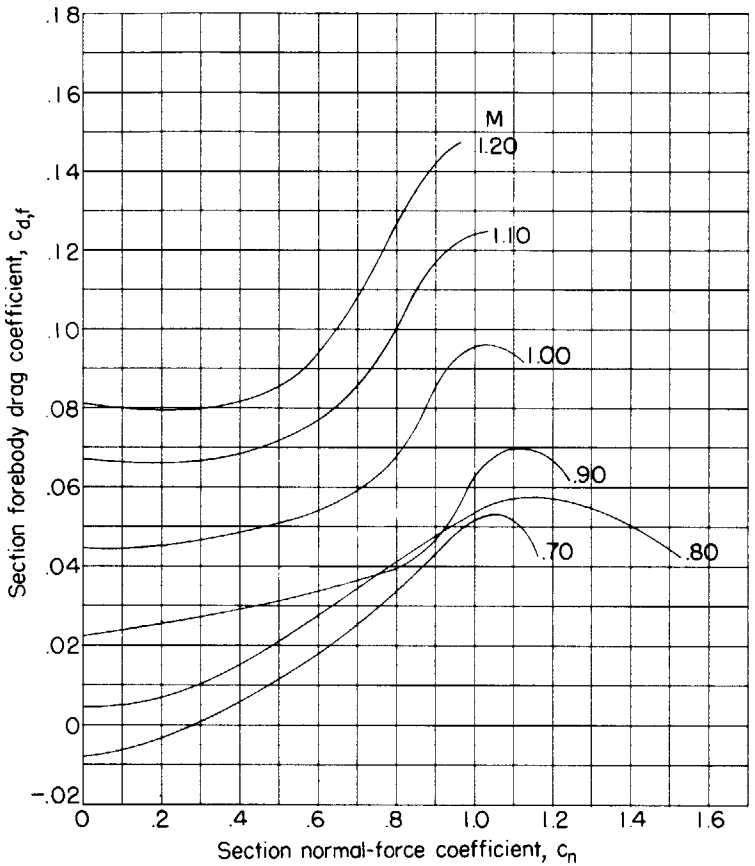

(a) Forebody drag coefficient.

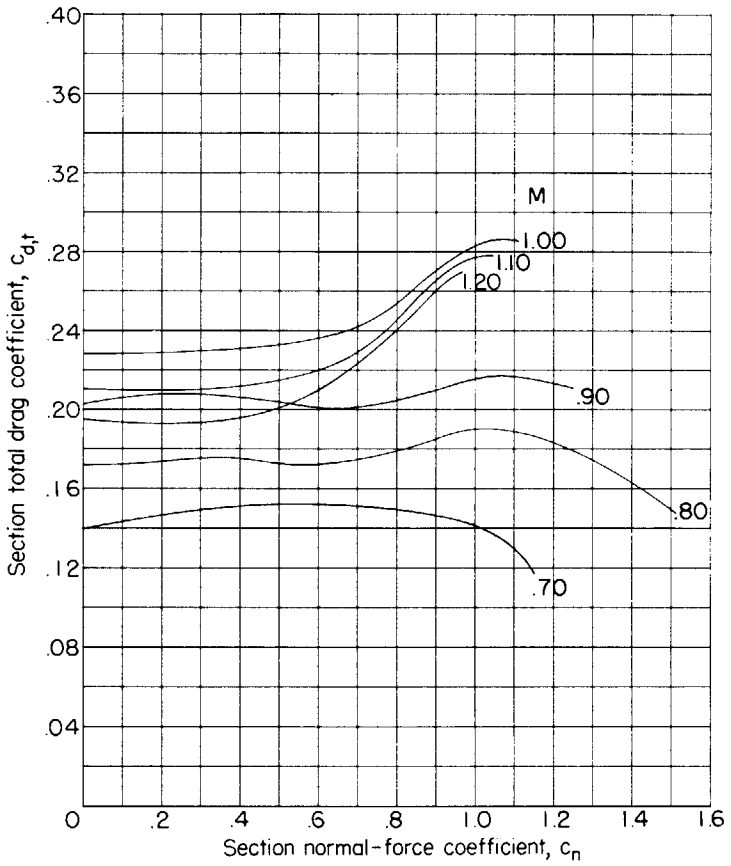

(b) Total drag coefficient.

Figure 11.- Variation of section drag coefficient with section normal-force coefficient at various Mach numbers for the sharp-leading-edge single-wedge airfoil.

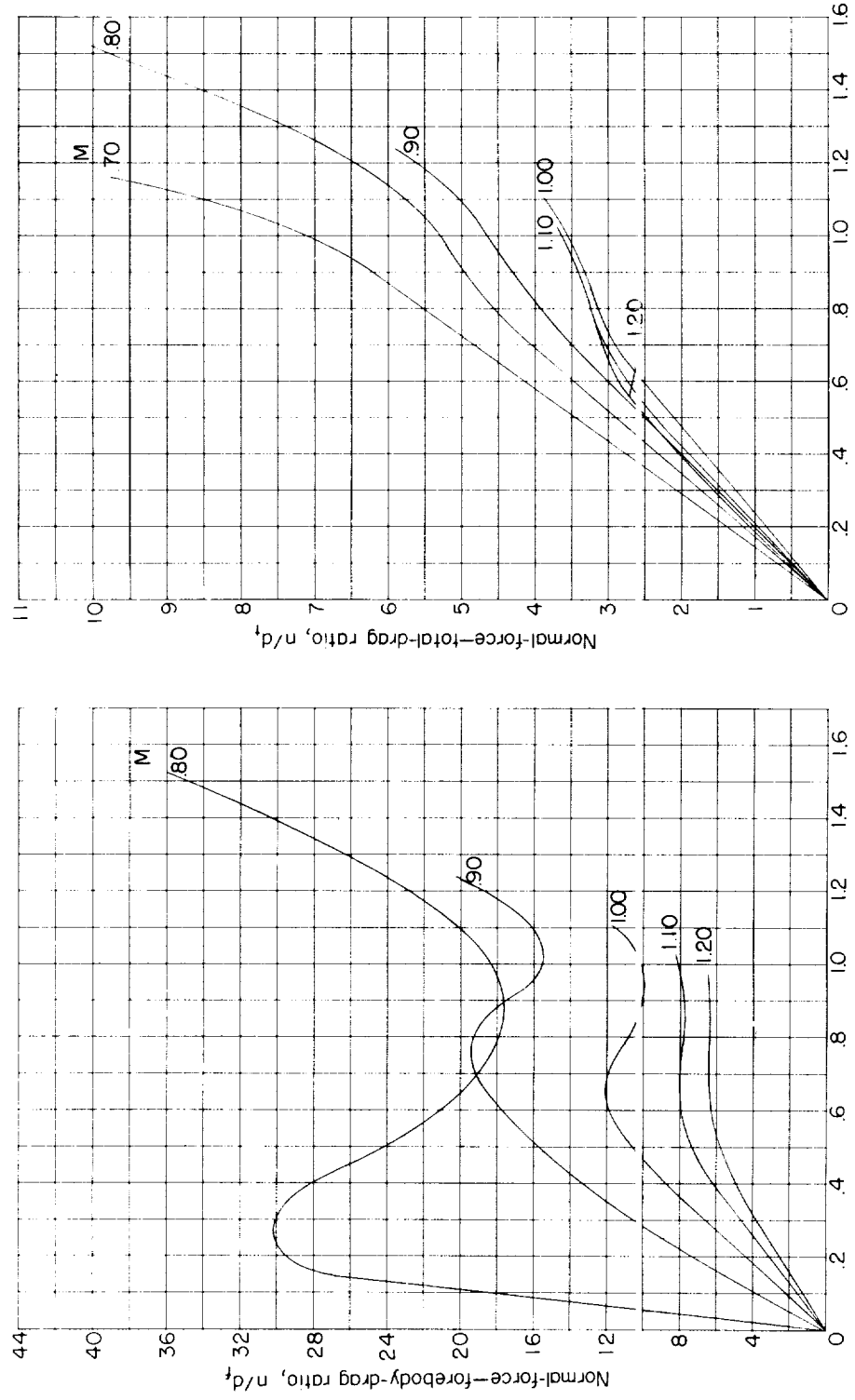

(a) Normal-force—forebody-drag ratios.

(b) Normal-force—total-drag ratios.

Figure 12.- Variation of normal-force—drag ratio with section normal-force coefficient at various Mach numbers for the sharp-leading-edge single-wedge airfoil.

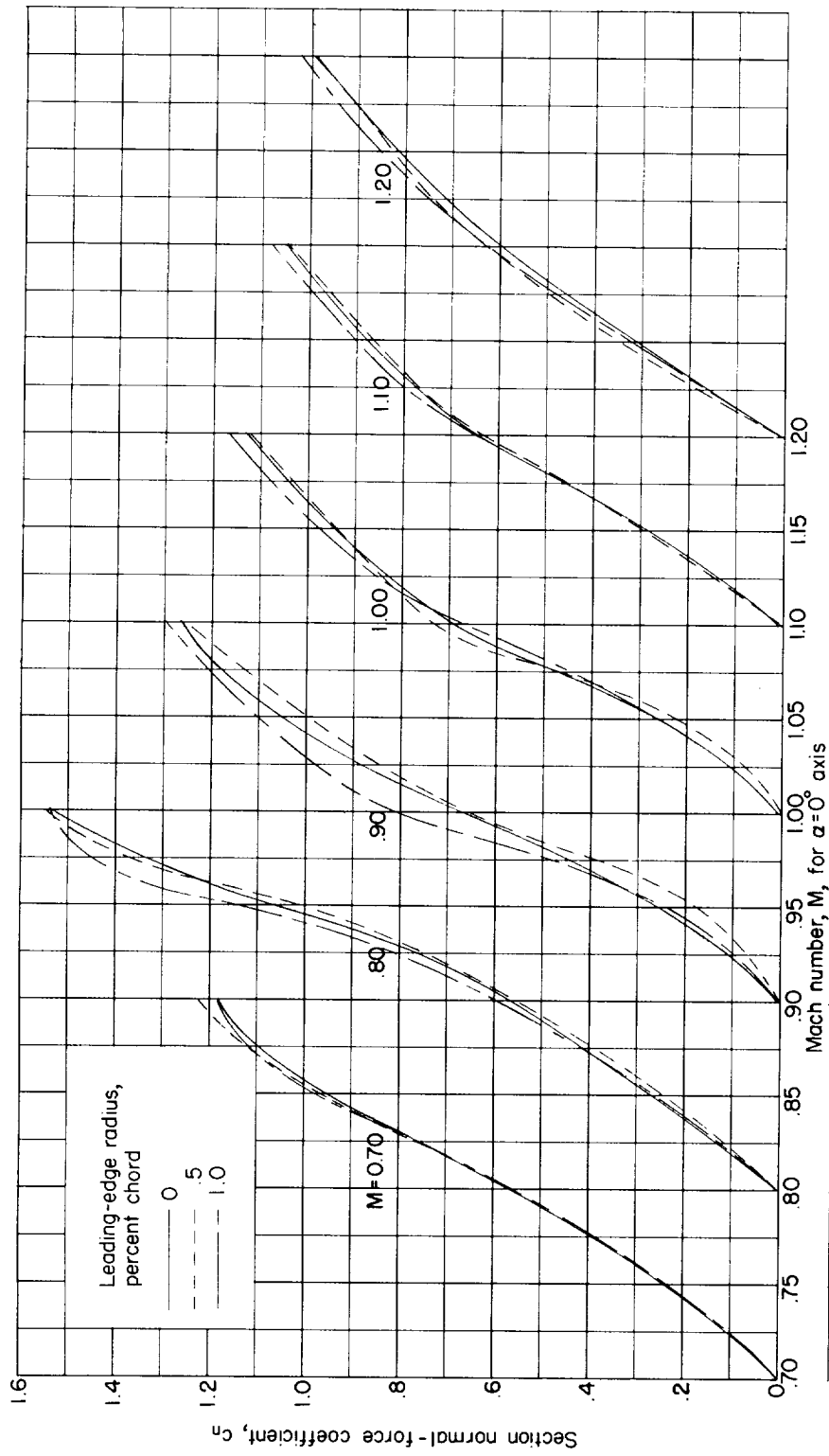

Figure 13.- Variation of section normal-force coefficient with angle of attack on the single-wedge airfoil for the three leading-edge radii.

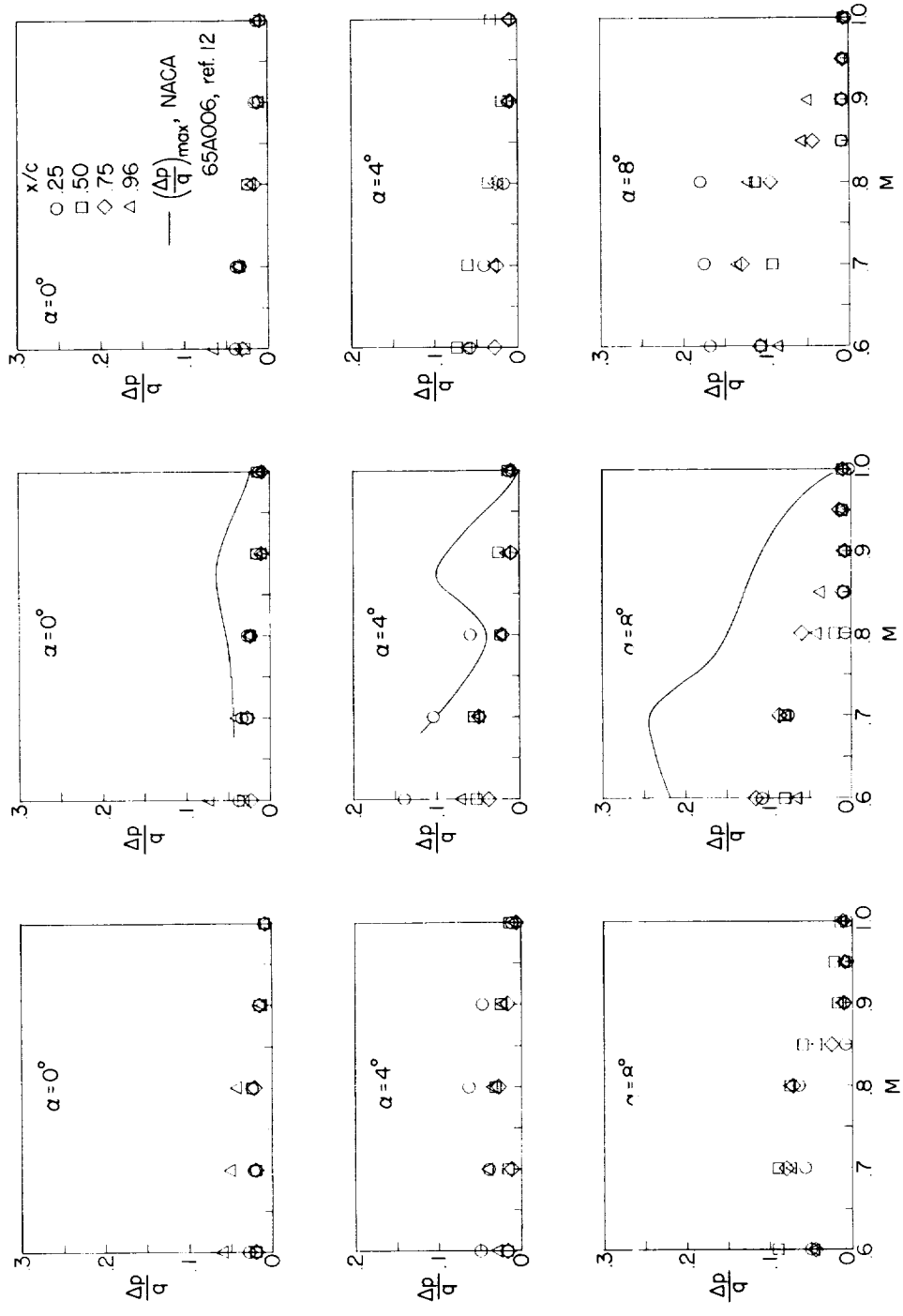

(a) r = 0 percent chord. (b) r = 0.5 percent chord. (c) r = 1.0 percent chord.

Figure 14.- Effect of Mach number, angle of attack, and leading-edge radius on the pressure pulsations over the upper surface of the single-wedge airfoil.

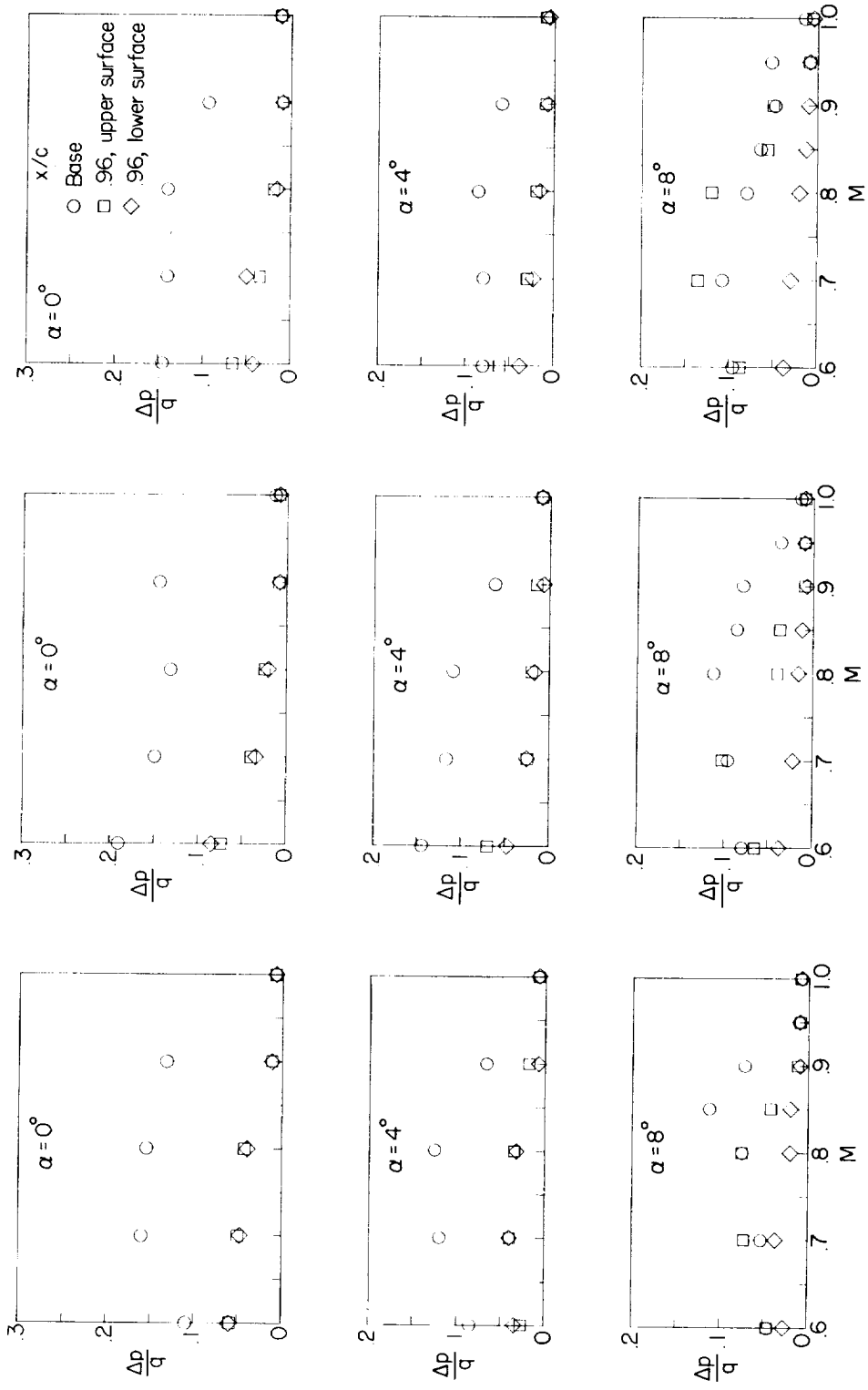

(a) r = 0 percent chord. (b) r = 0.5 percent chord. (c) r = 1.0 percent chord.

Figure 15.- Effect of Mach number, angle of attack, and leading-edge radius on the single-wedge airfoil on the base pressure pulsations.

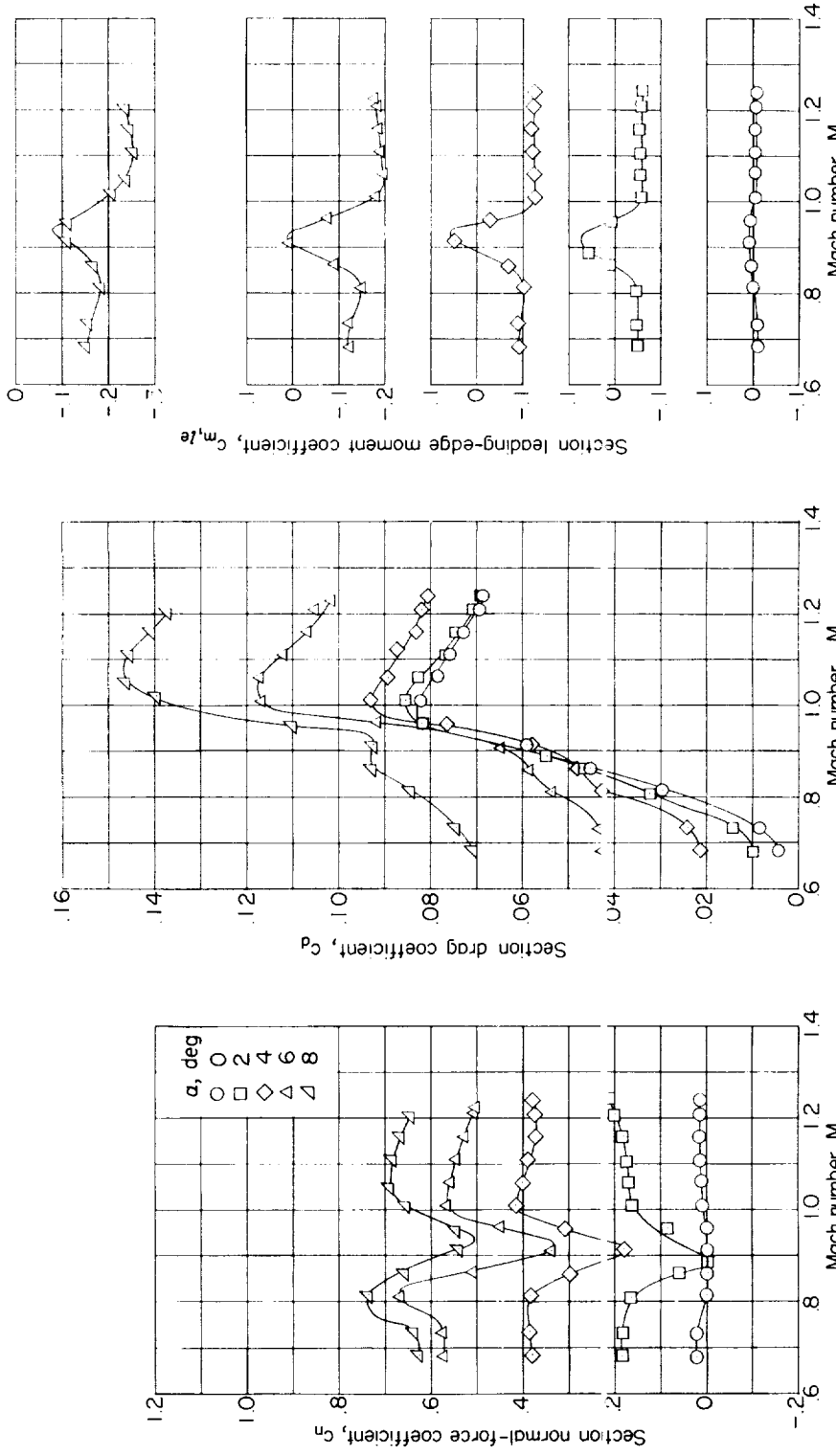

Figure 16.- Variation of section normal-force, drag, and leading-edge pitching-moment coefficients with Mach number for the diamond profile.

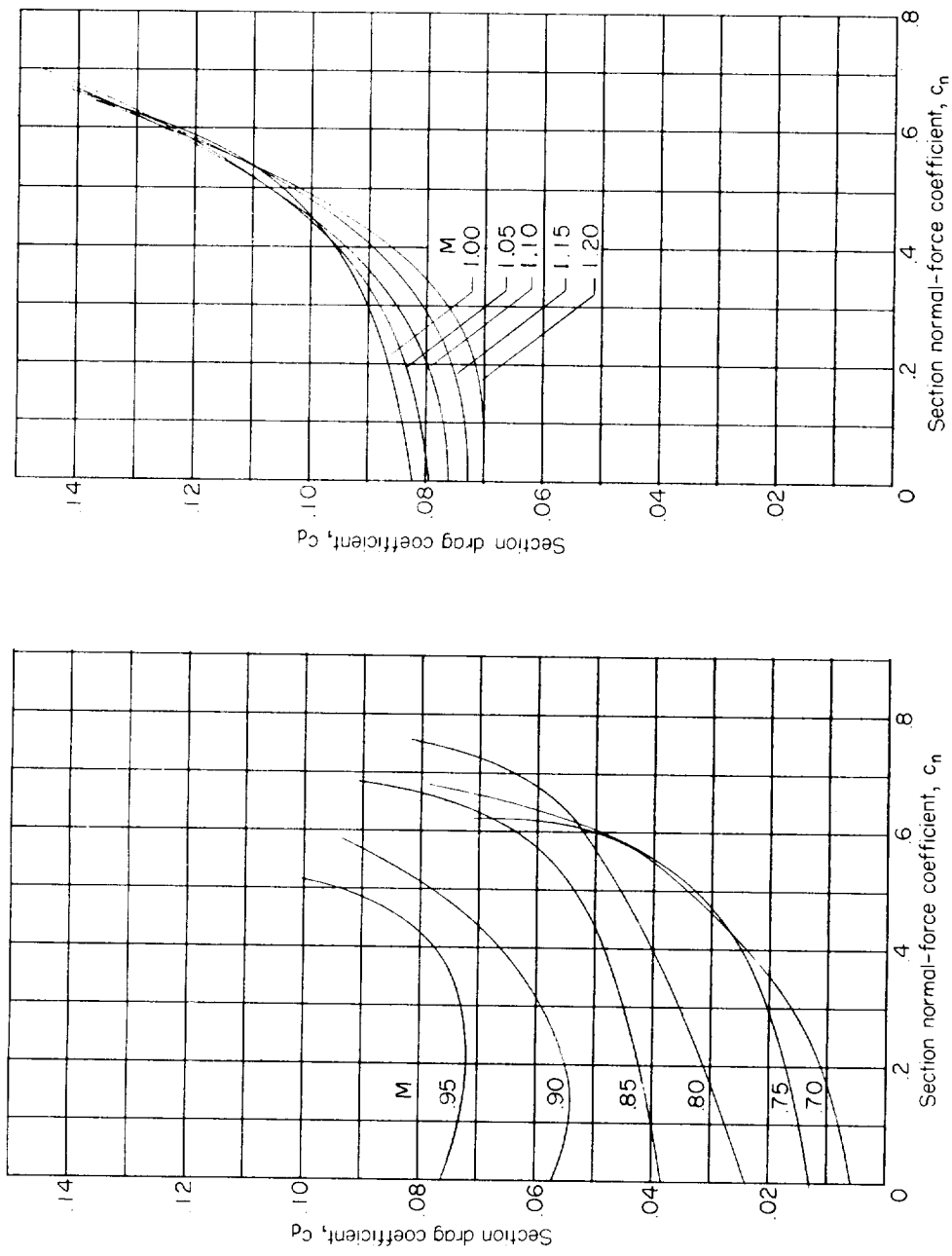

(a) Subsonic.

(b) Supersonic.

Figure 17.- Variation of section drag coefficient with section normal-force coefficient at various Mach numbers for the diamond airfoil.

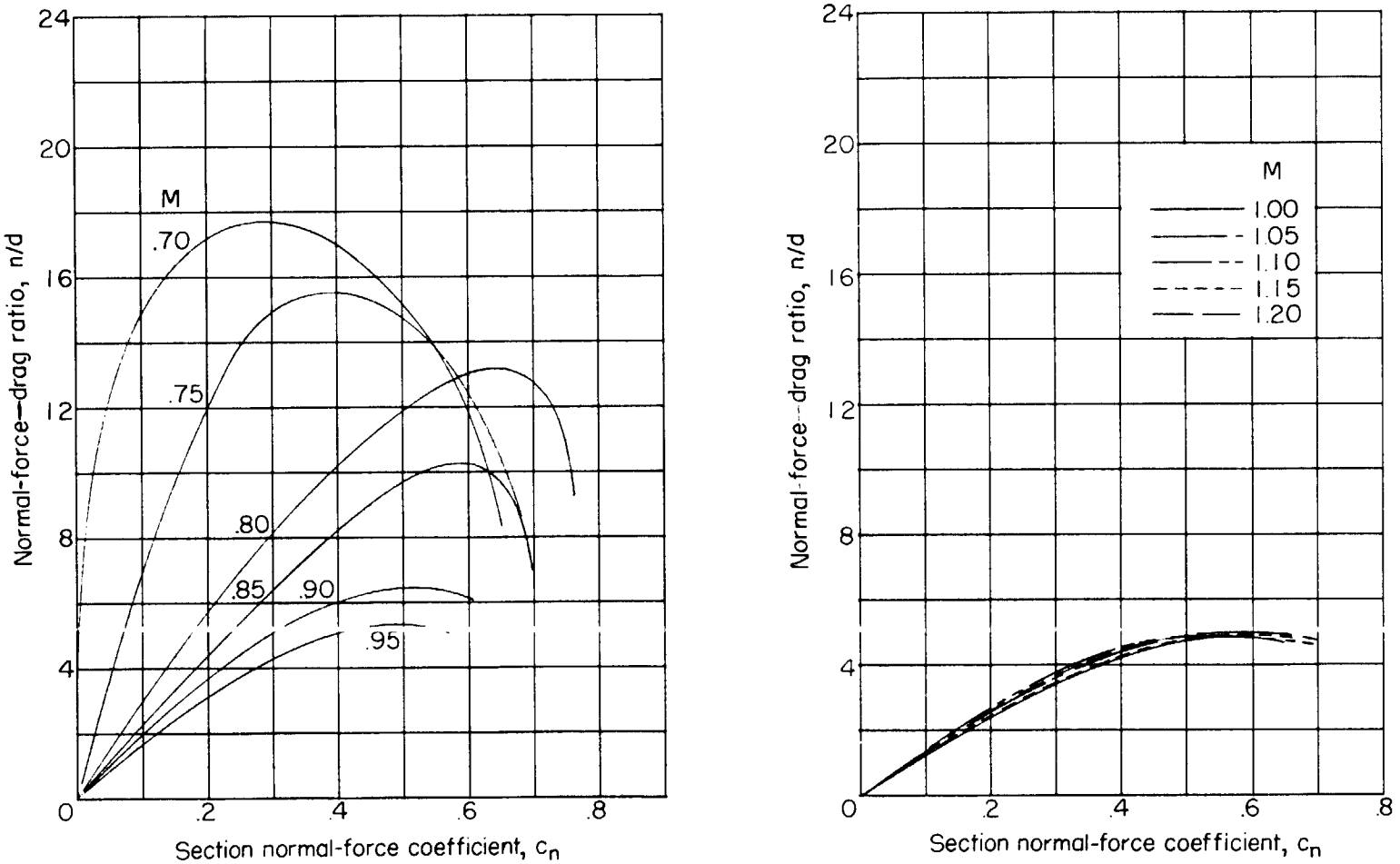

(a) Subsonic.

(b) Supersonic.

Figure 18.- Variation of section normal-force—drag ratio with section normal-force coefficient at various Mach numbers for the diamond airfoil.

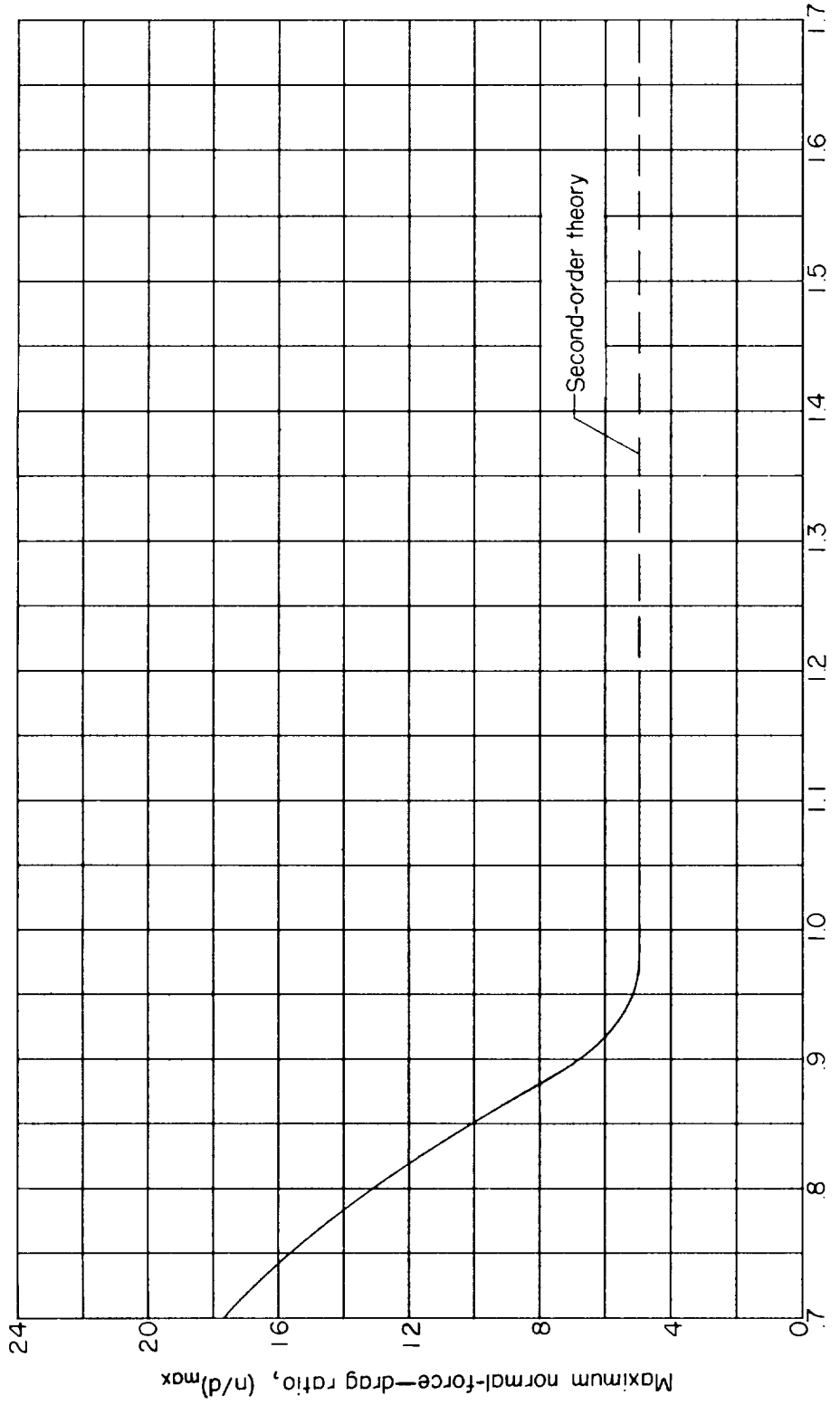

Figure 19.- Variation of maximum normal-force—drag ratio with Mach number for the diamond profile.

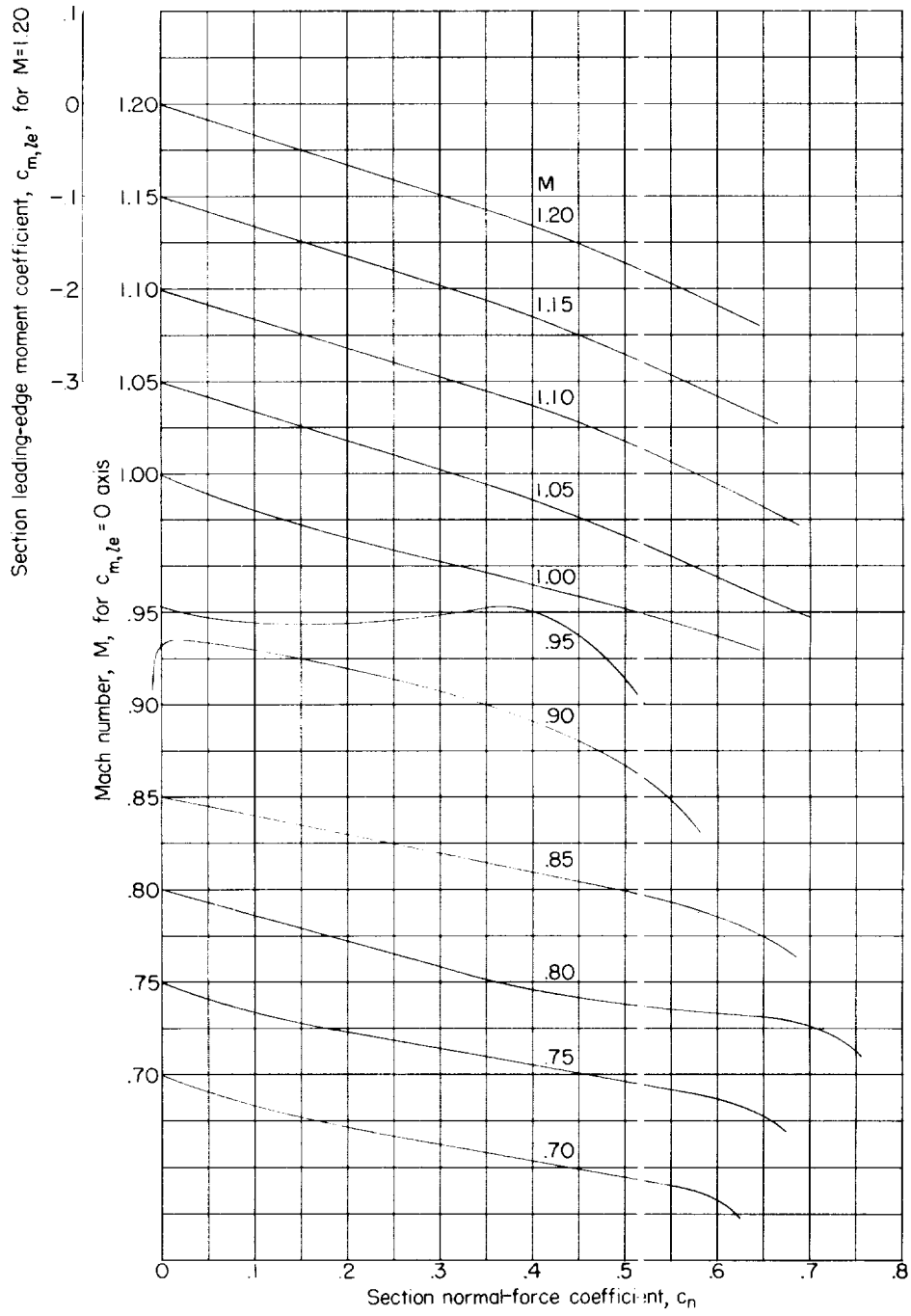

Figure 20.- Variation of section pitching-moment coefficient about leading edge with section normal-force coefficient at various Mach numbers for the diamond airfoil.

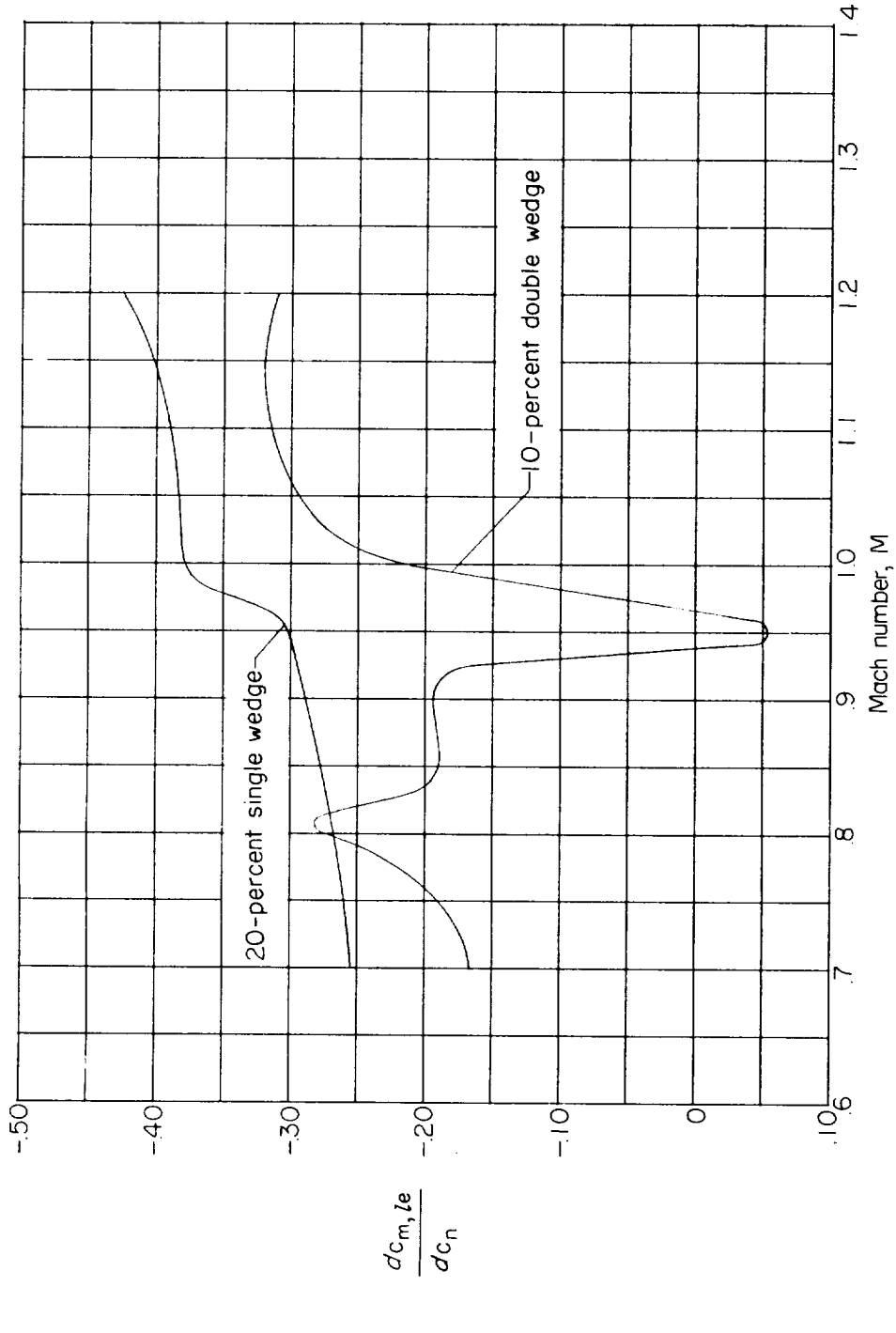

Figure 21.- Effect of Mach number on the stability parameter $\frac{dc_{m,le}}{dc_n}$ for the two airfoils tested. $c_n = 0.3$.

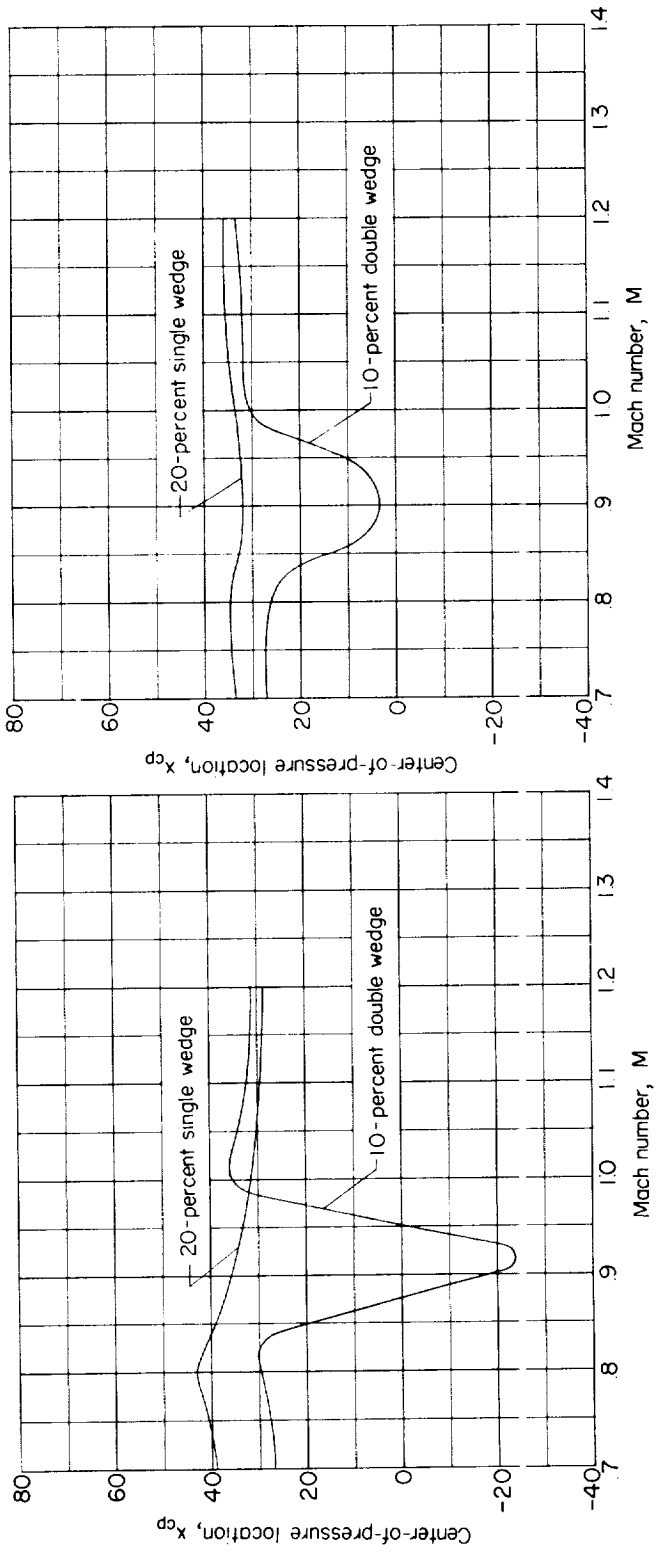

(a) $c_n = 0.2$.

(b) $c_n = 0.4$.

Figure 22.- Variation of center-of-pressure location with Mach number for the two airfoils.

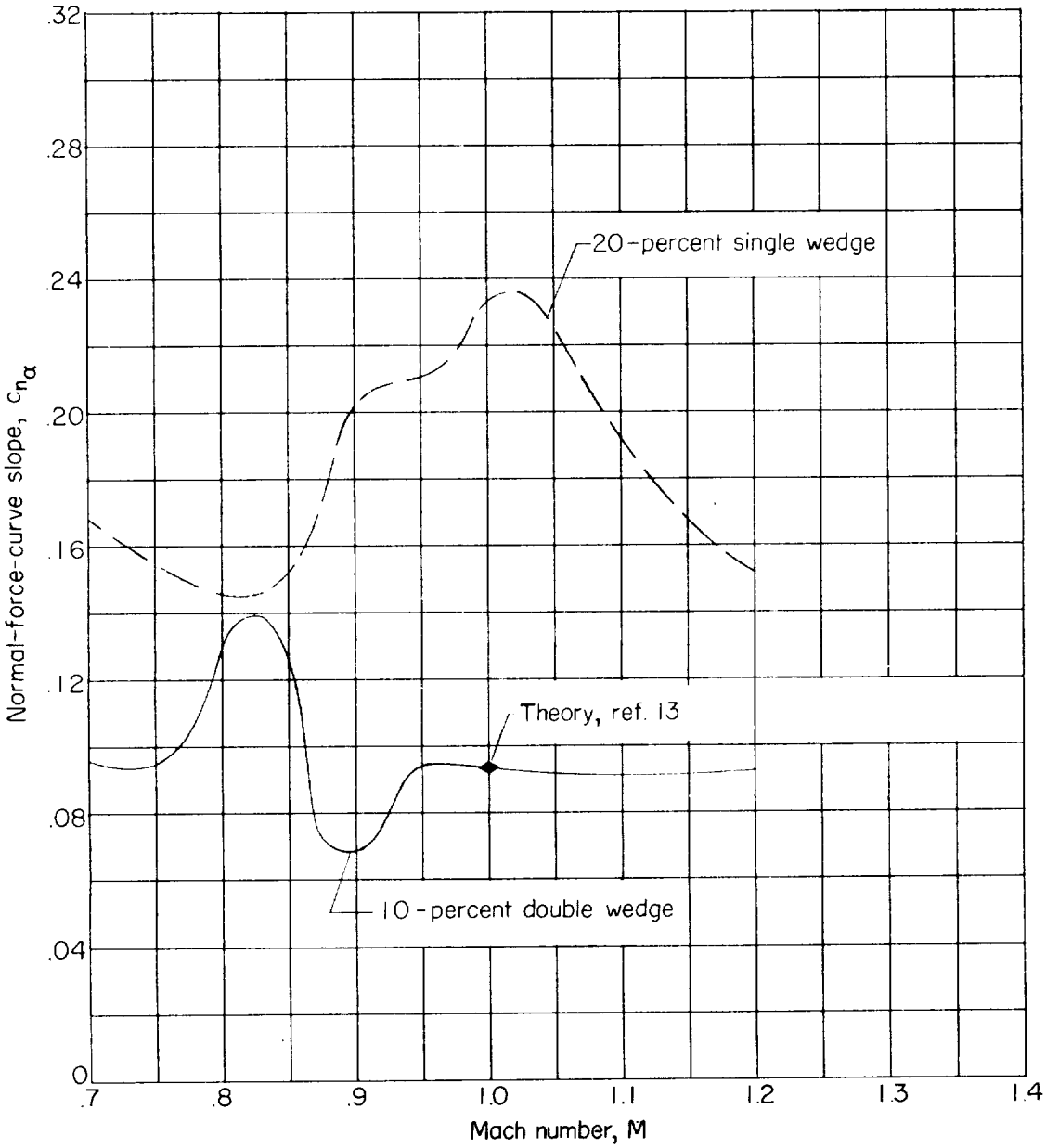

Figure 23.- Effect of Mach number on the section normal-force-curve slope of the sharp-leading-edge single-wedge airfoil and the 10-percent-thick diamond airfoil. $c_n = 0.4$.